63-3-4

Purdue University
Department of Physics

SEMICONDUCTOR RESEARCH
SEMIANNUAL REPORT

October 1, 1962 to March 31, 1963

Contract DA 31-124-ARO(D)-17

between
PURDUE RESEARCH FOUNDATION
and
ARMY RESEARCH OFFICE
PRF 3324

Purdue University
Department of Physics

SEMICONDUCTOR RESEARCH
SEMIANNUAL REPORT

October 1, 1962 to March 31, 1963

Contract DA 31-124-ARO(D)-17

between
PURDUE RESEARCH FOUNDATION
and
ARMY RESEARCH OFFICE
PRF 3324

PERSONNEL WORKING ON PRF 3324

October 1, 1962 - March 31, 1963

Research Staff:

H. Y. Fan, Principal Investigator
W. M. Becker*
R. Bray*
R. C. Buschert*
K. M. Ghanekar*
E. B. Hale*
H. M. James
E. J. Johnson*
V. A. Johnson*
W. Jung*
P. H. Keesom
P. H. Klose*
W. W. Lee*
M. P. Mathur*
G. S. Newell
N. Pearlman*
W. E. Pinson*
A. K. Ramdas*
L. M. Roth*
A. G. Sadasiv*
R. J. Sladek
D. L. Trueblood*
B. J. van der Hoeven

Service and Clerical Staff:

V. R. Bolyard*
S. S. Smith*
M. J. Ummel*

*Salary paid in part or in full by PRF 3324.

TABLE OF CONTENTS

I. ELECTRICAL AND OPTICAL PROPERTIES

HOT CARRIER DISTRIBUTION FUNCTION: EXPERIMENTAL DETERMINATION, DESCRIPTION, AND APPLICATION.

W. Pinson and R. Bray

I. Introduction

The amount of IR radiation transmitted through p-type Ge can be modulated by applying a strong electric field or by changing the temperature of the Ge. In both cases, the changes in transmission are attributable to a change in distribution function, hence a redistribution of the holes in the upper two valence bands. In the following both effects are combined to yield the energy distribution function of the hot carriers. The distribution functions have then been applied, with the aid of the low field transport parameters of the Ge, to compute a) the energy loss rates to optical and acoustic phonons, b) the hot carrier mobility, and c) a parameter describing the impact ionization rate for deep acceptors.

II. Energy distribution function of Hot Carriers

Fig. 1 shows the relevant parts of the band structure of Ge and the expression for the interband free carrier absorption as given by the theory of Kahn and Kane[1]. The IR absorption is due e.g. to a photon of energy $h\nu$ causing a hole at energy ϵ_{hh} in band 1, to jump vertically to band 3. Equation (1) on the figure shows that the absorption coefficient, α, is proportional to the square of the matrix element, H_{13}^2 for transitions from bands 1 to 3, to the hole density, p at ϵ_{hh} and inversely proportional to $h\nu$ and to f, a function of the curvature of the valence bands. The absorption coefficient may be modulated by changing p (ϵ_{hh}), either by applying a field to the Ge or by changing the temperature. If the other elements in equation (1) are independent of field and temperature, then the absorption coefficient at a given λ, depends only on the distribution function of the holes. For the measurement of absorption as a function of temperature, the temperature of the crystal changes slowly, the holes are always in thermal equilibrium with the lattice and thus have a Maxwellian distribution. When a pulse of high field is applied to the material the holes attain a steady state distribution but are not in thermal equilibrium with the lattice. As we shall see this steady state distribution is no longer Maxwellian.

Fig. 2 is a block diagram of the apparatus used to measure the change in transmission with field. IR from the monochromator is focussed on the Ge and then refocussed on the detector. A 5 μsecond long, high field pulse applied to the Ge causes the carriers to redistribute themselves in the upper valence bands (1 and 2)

and thus modulates the IR transmitted. The redistribution time is much faster than the rise time of the voltage pulse. The modulation shows up as a pulse on the detector and scope. The normally transmitted intensity "I_T" is measured in the same system by chopping the IR at 13 cps. All field measurements were made with Ge held at 77°K.

Fig. 3 shows the percentage modulation, "$\Delta I_T/I_T$" for fields of 130 and 2800 volts/cm the lowest and highest used. ΔI_T is the change in I_T caused by the field. The negative values are due to an increase of hole density far out in the heavy hole band; the positive values due to a decrease close to $\underline{k} = 0$. The ranges corresponding to 1 → 3 and 2 → 3 transitions are marked on the figure. Intensity modulation approaching 50% was observed. We have found that the percentage modulation also depends on the crystal orientation, on the direction in which the IR traverses the Ge and on the direction of polarization of the IR relative to the field direction.

Fig. 4 shows the change in absorption coefficient calculated from the percentage modulation for a field of 800 volts/cm. For comparison, we also show in this figure the change in absorption at zero field for a temperature increase of 100°K above the base temperature at 77°K. Comparison of the two curves shows qualitative but not quantitative agreement between the absorption coefficient changes due to temperature and field. This we attribute to the non-Maxwellian character of the field-perturbed distribution. Had the field simply heated the carriers to a higher "temperature", then the field curve would coincide with <u>some</u> temperature curve. No such correspondence could be found! The non-Maxwellian energy distribution of hot carriers may be obtained by properly correlating the absorption measurements $\alpha(T_L)$ made with varying temperature[2], and those made by applying electric field pulses, $\alpha(\vec{E})$. Use is made of the theory that the absorption coefficient at a given wavelength is proportional to the hole population at a specific energy in band 1, irrespective of whether the hole population is determined by varying the lattice temperature, or by the applied field. A simple proportion, as given in equation 2, then permits determination of the hole populations when the field is applied. Thus,

$$p_\lambda(\vec{E}) = p_\lambda(T_L) \cdot \alpha_\lambda(\vec{E})/\alpha_\lambda(T_L), \qquad (2)$$

where the hole population at any specific energy and known crystal temperature, $p_\lambda(T_L)$ is given by the Maxwellian distribution of Eq. 3 in the absence of applied field.

$$p_\lambda(T_L) \sim \frac{e^{-\epsilon_{hh}/kT_L}}{T_L^{3/2}} \qquad (3)$$

where p is carrier concentration, α is absorption coefficient, the subscript λ is the wavelength for which the particular quantities are determined, and $\bar{E}$ and T_L refer to electric field and temperature measurements respectively. It remains to specify what energy ϵ_{hh} in band 1 corresponds to the particular wavelength used. From the proportionality between p and α, and using the Maxwellian relation of Eq. 3, we obtain

$$\alpha_\lambda(T_L)\, T_L^{3/2} \sim e^{-\epsilon_{hh}/kT_L} \,. \qquad (4)$$

A semilog plot of $\alpha(T_L)\, T_L^{3/2}$ vs $1/T_L$ taken at selected wavelengths[2] yields the corresponding energy relations between ϵ_{hh} in band 1, and λ. An attempt at a similar analysis for band 2 was not successful, in that no distinguishing straight line slopes could be obtained at any λ.

Fig. 5 shows some calculated distribution functions for field strengths between 130 and 2150 volt/cm. The energy range between the dashed lines is that for which there is reliable data, i.e. for which application of Eq. 4 yields reasonably straight line slopes, hence values of ϵ_{hh}. The energy distribution for 800 volt/cm is shown again in Fig. 6, where it is compared with a Maxwellian distribution at 169°K, which has the same average energy as the 800 volt/cm distribution. The areas under the hot carrier, and the Maxwellian distribution curves are the same within experimental error. It is to be noted that the average energy is surprisingly low for such a large field strength. The non-Maxwellian character of the hot carriers is demonstrated[3]. Compared to a Maxwellian distribution, the hot carriers show a depletion of population at low and very high energies, and a piling up of carriers at intermediate energies, where the concentration becomes greater than can be found in a Maxwellian distribution at <u>any</u> temperature. The depletion at high energies is attributed to the large probability of emission of optical phonons of energy $k\theta_{opt.} = .037$ ev by those hot carriers with $\epsilon > k\theta_{opt}$.

III. <u>Application of Distribution Functions.</u>

A. Energy Loss Rate Calculation.

Two qualitative features stand out from the above results; (1) the non-Maxwellian character of the distribution of hot carriers, and (2) the low average energy even at strong electric fields. The latter result implies the presence of a very strong

energy loss mechanism which can only be attributed to strong interaction of holes with optical phonons. The deduction was quantitatively tested as follows: The energy loss rate for optical and acoustical phonon interactions was calculated utilizing the experimentally determined distribution function, represented by p(ε) in equation 5:

$$\left(\frac{d\varepsilon}{dt}\right)_{loss} = \int_0^\infty < \left(\frac{\delta\varepsilon}{\tau}\right)_{em} - \left(\frac{\delta\varepsilon}{\tau}\right)_{abs} > p(\varepsilon)\, d\varepsilon \qquad (5)$$

where the two terms in brackets represent the difference between energy loss and gain rates in emission and absorption processes; $\delta\varepsilon$, the amount of energy lost (or gained) by the hole in an interaction, is $k\theta_{opt}$ for optical phonon interactions, and $\hbar\omega$ for acoustical phonon interactions. The former is a constant, while the latter has to be taken as a function of scattering angle and carrier energy. The brackets indicate averaging over scattering angle where necessary. The collision time τ, different for the emission and absorption processes, requires knowledge of the appropriate deformation potentials for optical and acoustical phonon scattering. These were taken from previous analysis of the low field mobility[4]. The calculated energy loss rate may be compared with the experimentally measured one. The latter is equal to the energy gain rate of the carrier in steady state, which is just given by

$$(d\varepsilon/dt)_{gain} = q\,\mu\,\vec{E}^2\,p,$$

where μ is the measured mobility at given field, $\vec{E}$, and p is the total hole concentration.

Comparison of the measured and calculated results at various field strengths are shown in Fig. 7. The solid line is the experimental result. The energy loss rates calculated are indicated separately for optical and acoustical phonon interactions. It is seen that the calculated loss rate to optical phonons is very close to the measured total loss rate, and two orders of magnitude larger than the loss to acoustical phonons, which may indeed be neglected. The agreement is best where the distribution function is determined with the best precision, at about 800 volts/cm. The change in absorption was somewhat different for the sample oriented in the (100) and the (111) directions, so separate distribution functions were calculated for the two directions and the theoretical energy loss calculated for the resulting distributions. The power loss is slightly higher for the (111) than the (100) direction.

The optical phonon interaction had previously been introduced to explain the temperature dependence of the mobility of holes, but the strength of the interaction had been empirically determined to fit the data. The same parameter now enables us to account quantitatively for the carrier power loss and the relatively low average energy of the hot hole distributions.

B. Impact Ionization Rate of Deep Lying Acceptors

The distribution curves show relatively few carriers at energies much above $k\theta_{opt}$. Thus it should be difficult to ionize impurities with deep-lying levels, ϵ_I. This has already been observed experimentally[5]. We can look at this more quantitatively as follows. We assume that the ionization cross section per carrier, σ, is proportional to the difference between the ionization threshold and the carrier energy. The ionization rate is also proportional to the carrier velocity, $v \propto \sqrt{\epsilon}$. If the product $\sigma v \propto (\epsilon - \epsilon_I)\sqrt{\epsilon}$ is now averaged over the distribution function $p(\epsilon)$ from ϵ_I to ∞ (see equation on Fig. 8) the result is a value A_I which is proportional to the impact ionization rate. The same product, σv, may be averaged over Maxwellian distributions at several temperatures. A temperature with its accompanying Maxwell distribution may thus be found which has the same impact ionization rate A_I as that for each of the experimentally determined field distributions. This equivalent temperature as a function of field strength is shown in Fig. 8 for two different deep lying acceptors, Zn and Cu. The equivalent temperature is quite low and changes only slowly with increasing field. It is quite similar for both acceptors, being a little higher for the Zn than for the Cu, as expected. Experimentally it was found[5] that it was somewhat more difficult to ionize Cu than Zn impurities. To explain completely the difficulty of ionizing deep lying acceptors in Ge, it is necessary to consider other factors than just the effective temperature of the hot carriers for ionization. Thus the recombination mechanism is an equally important factor. However, the equivalent temperatures for ionization obtained from the above analysis are much lower than had been anticipated previously and must be considered a major factor in the observed behaviour.

C. Hot Carrier Mobility

The energy distribution functions were used to calculate the mobility of the hot carriers. Previously the mobility of the hot carriers had been calculated using a Maxwellian distribution function with elevated carrier temperatures - a procedure which had given poor agreement with the experimental mobilities[6]. The calculations made with the new distribution function were equally poor, as shown in Fig. 9. In order to explain why the energy loss calculations give good agreement between theory and experiment while the mobility calculations do not, the factors going into each

need to be compared. The energy loss rate depends only on the energy distribution function of the hot carriers. The mobility calculation depends on the momentum distribution function. It is the former and not the latter which is measured, and the problem is how to deduce the momentum distribution function $f(\bar{k})$ from the measured energy distribution function $f(\epsilon)$. $f(\epsilon)$ is obtained from the distribution $p(\epsilon)$ by a density of states factor, $\propto \sqrt{\epsilon}$. The assumption was made that the measured distribution function was essentially isotropic, and that the perturbation due to the field was linear, and given by the usual relationship,

$$f(\bar{k}) = f_o - e \bar{E}_x \tau v_x \frac{\partial f(\epsilon)}{\partial \epsilon} , \qquad (6)$$

where $\partial f/\partial \epsilon$ was evaluated by determining the slopes at various energies of the experimental determined $f(\epsilon)$ curves. A criterion for the validity of this approximation is that the perturbation be small compared to the <u>isotropic</u> term f_o (which need <u>not</u> be the same as the undisturbed distribution at zero field strength). The criterion can also be approximated by the condition: $v_{drift} \; \tilde{v}_{thermal} \ll 1$. When, however, v_{drift} is calculated from the measured mobility, and $\tilde{v}_{thermal}$ from the average energy of the experimental distribution functions, it turns out that the ratio is of the order of 1/2, clearly violating the assumption of linearity of the perturbation of the distribution function.

A second difference between the power loss and the mobility calculations is that the former depends only on the optical mode collision time, while the latter depends on acoustical, optical, and ionized impurity relaxation times. However, we do not consider this difference to be responsible for the difficulties.

It is of interest to consider the reason for the large ratios of $v_{drift}/\tilde{v}_{thermal}$, and the consequences of it. The large values of the ratio can be attributed to the strong inelastic scattering in p-type germanium, which is just due to the optical phonon interaction. Because of the large energy loss rate, the carriers can not become very hot, so $\tilde{v}_{thermal}$ remains relatively low. The drift velocities however become high as the field is increased. The carriers then have a strong element of streaming rather than diffusive motion. The implication is that the momentum distribution of the carriers is strongly displaced away from $\bar{k} = 0$ in the direction of the field. An interesting consequence of such <u>non-linearly displaced</u> distributions is that the absorption of the IR light should depend on the direction of polarization, thus making the Ge dichroic when the carriers are hot. We have looked for and observed such an effect and are in the process of investigating it in more detail.

1. A. H. Kahn, Phys. Rev. 97, 1647 (1955); E. O. Kane, J. Phys. Chem. Solids 1, 83 (1956).
2. See W. Pinson and R. Bray, Purdue Prog. Report No. 6, Jan.-March (1962).
3. See M.A.C.S. Brown, E.G.S. Paige and L.N. Simcox, International Conf. on Physics of Semiconductors, Exeter (1962), for a similar study limited to much lower electric field strengths, at T = 93°K.
4. D. Brown and R. Bray, Phys. Rev. 127, 1593 (1962).
5. D. Brown and R. Bray, Bull. Amer. Phys. Soc., March, 1962 (Monterey Meeting).
6. D. Brown and R. Bray, Proceedings of the International Conf. on Semiconductor Physics Prague, (1960), (Czech. Acad. Sciences, Prague) P. 82.

OSCILLATORY MAGNETORESISTANCE OF GaSb

W. M. Becker and H. Y. Fan

Previous measurements[1] on n-type GaSb(Te) showed that at low temperatures the transverse magnetoresistance is small for low carrier concentrations, and rises sharply at an $n_c \sim 1.2 \times 10^{18}$ cm^{-3} where conduction in a $< 111 >$-valley band sets in. These measurements were carried out to 14 kilogauss. Measurements made during this period extended the range of investigation to 30 kilogauss.

For samples with Fermi levels close to the upper band edge, the measurements reveal single-period Shubnikov-de Haas oscillations in both the transverse and longitudinal magnetoresistance. The transverse and longitudinal oscillations are in phase for each sample, and the period is given by the zero field Fermi energy. Curves showing behavior typical of samples having concentrations $n_c \sim 1.2 \times 10^{18}$ cm^{-3} are presented in Figure 10. The amplitude of the oscillations increases sharply near this concentration. The average component of the transverse oscillations increases proportional to H^2; $(\Delta\rho/\rho H^2)$ transverse also increases sharply at $n_c \sim 1.2 \times 10^{18}$ cm^{-3}. The results for a number of samples are summarized in Figure 11. Using an effective mass of 0.052 m_o for the center band, the oscillation at 30 kilogauss is found to correspond to quantum level ~ 10 for the samples investigated.

Since both the transverse magnetoresistance and the oscillation amplitudes increase sharply over the same range of values of the Hall coefficient, the oscillations appear to be correlated with the onset of conduction in the higher lying $< 111 >$ valleys. Other measurements[1] show, however, that the 4.2°K Hall mobility rises with concentration, suggesting that the quantum condition, $\omega\tau \sim 1$, may not be satisfied at low concentrations for carriers in the center band.

For uniaxial compressional stress along the < 111 > direction, it is expected that there will be a relative shift of one of the < 111 > valleys toward the central minimum. If the effects discussed above depend on the position of the Fermi level with respect to the higher lying < 111 > valleys, the following behavior would be expected: (1) a shift in the oscillations toward lower fields, (2) an increase in the average component of the transverse oscillations, and (3) an increase in the amplitude of the oscillations. The first two effects are clearly indicated for a sample with $R_{4.2^oK} = -5.49$ cm^3/coulomb as shown in Figure 12, but no appreciable change is noted in the oscillation amplitude. The shift of the oscillations corresponds to a relative decrease in energy between the center band minimum and one of the < 111 > valleys of $\sim 1 \times 10^{-3}$ ev for $X \doteq 3 \times 10^8$ dynes/cm^2.

The results on both the transverse magnetoresistance, the oscillatory behavior, and the pressure effects are all consistent with a picture of alternating shift of carriers from one band to another with changing field. However, calculation gives only $\sim 1.2\%$ shift of carriers from one band to another for the quantum level involved whereas the experimentally observed variation is much greater (x 10 at 30 kilogauss). Other mechanisms must therefore also be considered to account for the effects.

---

1. W. M. Becker, A. K. Ramdas, and H. Y. Fan, J. Appl. Phys. 32, 2094 (1961).

GALVANOMAGNETIC EFFECTS IN HEAVILY DOPED P-TYPE GERMANIUM

G. Sadasiv

The Hall effect and magnetoresistance in several samples of germanium with gallium impurity concentrations ranging from 6×10^{17} to 6×10^{18} cm^{-3} have been measured. The measurements were made at 78°K, 4.2°K, and 1.3°K; with magnetic fields ranging up to 30 kG.

We first discuss the results obtained at 78°K. The values of the resistivity, and the Hall coefficient at very low fields, for the different samples are given in Table I. The direction of the current, and the plane in which the magnetic field was rotated in making the magnetoresistance measurements, are also indicated in the Table.

TABLE I $T = 78^{\circ}K$

Sample	R_o $cm^3\ coul^{-1}$	ρ_o ohm cm	< i >	< H > ⊥ to
I a	8.46	.0139	< 100 >	< 100 >
b			< 110 >	< 001 >
II a	5.87	.0106	< 100 >	< 011 >
b			< 110 >	< 001 >
III a	4.13	.0081	< 100 >	< 100 >
b			< 110 >	< 001 >
IV a	.95	.0026	< 100 >	< 011 >
b			< 110 >	< 001 >

No longitudinal magnetoresistance was detected in any of the samples. The transverse magnetoresistance data for the samples (a) are given in Fig. 13. Here $\Delta \rho/\rho H^2$ is plotted as a function of H. The data for the samples (b) were, within experimental error, the same as those for the samples (a). As can be seen $\Delta \rho/\rho$ is approximately proportional to H^2, though saturation effects are clearly apparent in the purer samples.

These experimental results have been analyzed on the basis of the following model. The structure of the valence band in pure germanium is known from cyclotron resonance experiments. We assume that in the heavily doped material the band structure is unaltered, and that there are no localized states, so that we have N_A holes in the normal valence band. There are two types of holes, the heavy holes with $m^* = .36\ m_o$, and light holes with $m^* = .044\ m_o$. The ratio of the number of heavy holes to the number of light holes is $p_h/p_\ell \approx 24$. The orientation dependence of the magnetoresistance suggests that the warping of the bands may be neglected, so that they can be treated as simple spherical bands. It is also assumed that the scattering mechanism is the same for both types of holes, and that the relaxation time $\tau \propto \epsilon^s$, where ϵ is the energy of the carrier; the constant of proportionality is different for the two types of holes. Simple transport theory can then be used to calculate the magnetoresistance. For the samples that we are considering neither the non-degenerate nor the completely degenerate approximations can be made in calculating the transport coefficients, the exact Fermi integrals were therefore used in the computations.

We denote the ratio of the conductivity mobilities for the two types of holes by α. The best fit to the data is obtained for a value of $\alpha \approx 3$, and $s = 3/2$. This is the result one would expect if the scattering were due to ionized impurities. The

observed variation of Hall coefficient with magnetic field is also consistent with the simple model. The values of R as a function of H^2 for sample II are given in Fig. 14.

The assumptions made indicate that $R_o pe \approx 2$. Actual chemical analysis on similar specimens by Bernard et. al.[1] indicate that this is indeed the case if $N_A < 10^{19}$ cm^{-3}.

The model is, of course, an oversimplified one; and the experimental results are not accurate enough to decide whether this is the only possible interpretation of the data. Measurements were therefore made at 4.2°K and 1.3°K. In this case one would expect that the samples would show complete degeneracy, and a smaller magnetoresistance effect would be seen. The experimental results, however, were completely at variance with expectation. The transverse magnetoresistance at 4.2°K was larger than at 78°K; and showed a linear dependence on field rather than a quadratic one. A longitudinal magnetoresistance was also observed which was comparable to the transverse one for fields up to 6 kG, and then showed signs of saturation at higher fields. The results are shown in Fig. 15. The behavior of the samples (b) was the same as that of the samples (a).

The Hall coefficient also varied more rapidly with field at 4.2°K than at 78°K. The values of R as a function of H^2 for sample II are shown in Fig. 14.

At 1.3°K the magnitude of the magnetoresistance effect increased. The results for sample II are given in Fig. 16.

Keesom and Seidel[2] have measured the heat capacity of heavily doped p-type material in the temperature range from 0.5°K to 4.2°K. Their results are in agreement with the predictions of the simple degenerate gas model. Thus we must conclude that though the magnitudes of R_o and ρ_o change only slightly in going from 78°K to 4.2°K, the scattering mechanism is different at the two temperatures.

---

1. W. Bernard, H. Roth, and W. D. Straub, Bull. Am. Phys. Soc. 8, 224 (1963).
2. P. H. Keesom and G. Seidel, Phys. Rev. 113, 33 (1959).

PIEZORESISTANCE OF n-GaAs

R. J. Sladek

Piezoresistance measurements were begun previously[1] on oriented single crystal specimens of n-type GaAs in order to determine whether or not they would indicate appreciable conduction in subsidiary minima not located at $\underline{k} = 0$ since, recently, magnetoresistance measurements of Kravchenko and Fan[2] revealed anisotropy in magneto-

resistance which could be explained as due to there being appreciable conduction in (100) type minima.

We have continued the piezoresistance investigation by measuring the piezoresistance of a number of samples as a function of temperature between 77°K and 300°K. The samples had apparent carrier concentrations at room temperature between 8×10^{14} cm^{-3} and 3.7×10^{16} cm^{-3} and were oriented with the long dimension in the [100], [110], or [211] direction. Uniaxial compression and measuring current were applied along this dimension and the piezoresistance was measured along it except as indicated.

The longitudinal piezoresistance as a function of temperature for a number of samples is plotted in Fig. 17 in which π is actually the relative change of resistance per unit uniaxial compressive stress. (The numbers on the curves indicate the carrier concentration at room temperature, e.g. 1.5 - 10^{15} means 1.5×10^{15} carriers/cm^3.) From Fig. 17 it can be seen that: (1) π decreases with increasing carrier concentration, and (2) the samples fall into two groups each having a different kind of temperature dependence for π. One group exhibits a monotonic increase with decreasing temperature and the other group exhibits a minimum below room temperature. The position of the minimum depends on carrier concentration and moves to higher temperatures as the carrier concentration increases. If this pattern holds for even higher concentrations the negligible π measured by Sagar[3] on a sample with a somewhat greater concentration than our highest concentration is quite consistent with our results.

The kind of temperature dependence exhibited by π can be correlated with the behavior of the Hall coefficient, R_H, as a function of temperature which is plotted in Fig. 18. (A field of 4500 gauss was used for the data.) From Fig. 18 it can be seen that the samples again fall into two groups. For one group $|R_H|$ increases very greatly with decreasing temperature and it is these samples which have a large π which is monotonic with temperature. For the other group $|R_H|$ increases only slightly as temperature goes down and these are the samples in which π goes through a minimum as a function of temperature.

In order to elucidate the origin of the piezoresistance, the effect of crystal orientation was studied. π was found to be quite insensitive to crystal orientation. For example, for a [100] length sample and a [110] length sample each having about 1.8×10^{15} carriers/cm^3 (at room temperature) it was found from the longitudinal effects that $\pi_{11} = 65 \times 10^{-12}$ cm^2/d and $\frac{1}{2}(\pi_{11} + \pi_{12} + \pi_{44}) = 67 \times 10^{-12}$ cm^2/d and that from the transverse voltage with longitudinal current and stress $\pi_{44} \approx 5 \times 10^{-12}$ cm^2/d. Combining these results $\pi_{11} - \pi_{12} = 1 \times 10^{-12}$ cm^2/d. Thus both shear coefficients π_{44} and $\pi_{11} - \pi_{12}$ are very small compared to π_{11}. This indicates that the large

longitudinal piezoresistance effects are not due to transfer of electrons between multivalley minima and hence conduction must be overwhelming in the minimum at $\underline{k} = 0$.

(Orientation effect data were also taken on samples of the group showing a minimum in π vs T with the same type of results as for the 1.8×10^{15} cm^{-3} samples.)

Finally we measured the effect of stress on the Hall coefficient (at 4500 gauss) for samples in both groups. In all cases

$$\frac{\Delta \left| R_H \right|}{\left| R_H \right| X} = \pi_{Hall} \approx \pi_{long.}$$

Thus the piezoresistance seems to be due to a decrease in carrier concentration with increasing uniaxial compression. Probably the most likely explanation is a change in the ionization of deep donor levels due to the conduction band edge moving away from them due to the applied stress. The two types of temperature dependence for the piezoresistance may be a consequence of different kinds of compensation plus different proportions of shallow to deep donor levels.

Thermoelectric power measurements are planned to check this last notion by locating the Fermi level. Piezoresistance measurements using hydrostatic pressure are also planned to obviate the transverse measurement needed when only uniaxial stress is used.

---

1. R. J. Sladek, Semiconductor Research Eighth Quarterly and Final Report, Oct. 1, 1961 to Sept. 30, 1962.
2. A. F. Kravchenko and H. Y. Fan, Rept. of Intl. Conf. on Physics of Semicond. Exeter 1962, p. 737.
3. A. Sagar, Phys. Rev. 112, 1533 (1958).

OPTICAL PROPERTIES OF III-V SEMICONDUCTOR COMPOUNDS

E. J. Johnson and H. Y. Fan

Infrared measurements at $1.5^{\circ}K$ show a step on the absorption edge of InSb. Under applied magnetic field the step develops into a peak which moves to higher photon energy and splits into two components[1]. This behavior can be described approximately by:

$$(h\nu)_{\pm} \approx (Eg - \epsilon) + \frac{1}{2} (\hbar \omega_c \pm g_c \beta_o H)$$

where:

1) $(h\nu)_+$, $(h\nu)_-$ are the photon energies of each peak.

2) ϵ = .006 ev

3) ω_c is the cyclotron frequency of electrons.

4) g_c is the g-factor for spin splitting in the conduction band.

In analogy to previous work on GaSb[1] the absorption was attributed to transitions involving an ionized acceptor level and the conduction band. Related bound exciton absorption may be present, particularly with applied magnetic field. Recent measurements (Fig. 19) demonstrate that the strength of the absorption is, indeed, related to impurity concentration. Further, the following considerations show that the impurity level involved is one near the valence band. 1) The threshold for the absorption occurs at $h\nu \lesssim Eg - .006$ ev. The related ionization energy is then $|E_I| \gtrsim .006$ ev. Therefore the level lies between E_{CB} - .006 and E_{VB} + .006. 2) The absorption is observed in degenerate n-type material, therefore, with the Fermi level in the conduction band. 3) The absorption is observed in p-type samples with the Fermi level near E_{VB} + .006 ev. Any level between E_{CB} and E_{VB} + .006 ev will be in different charge states in the respective samples and cannot give rise to the same absorption. Therefore the level is near the valence band - either an ionized acceptor or a neutral donor. The level is probably an ionized acceptor, possible Zn.

The absorption edges of various other III-V compounds and silicon have been surveyed at 1.5°K for bound exciton and impurity absorption.

GaAs shows a step in absorption at about 1.495 ev which is probably related to an impurity level of about .023 ev. This step is not significantly affected by magnetic fields as high as 22 kG. This step in absorption has been observed by others[2,3]. Nathan[3] sees, in addition, a peak in emission apparently associated with the reverse transition.

InP has a slowly rising tail on the absorption edge of about the same magnitude at both room temperature and 1.5°K. At the lower temperature several steps occur which are insensitive to a magnetic field of 22 kG. The steps are probably associated with impurity absorption. The absorption rises sharply to beyond 10,000 cm^{-1}. Very thin samples are necessary for measurement at shorter wavelengths.

InAs displays a sharply rising edge from an absorption of 2 cm^{-1} to about 1000 cm^{-1}. This may be the intrinsic absorption edge or, more likely, the threshold for impurity or bound exciton absorption.

The absorption edge in silicon begins with indirect transitions and should present an excellent situation to study bound exciton transitions. These can take place without phonon participation and appear, therefore, in a region of the spectrum

where no band gap transitions occur. Haynes[4] has observed strong emission peaks in silicon which he attributes to excitons bound to neutral impurities. Attempts were made to observe the corresponding absorption. Samples with impurity concentrations (B) as high as 3.3×10^{17} cm^{-3} were examed. No such absorption was observed although the background absorption was less than .02 cm^{-1}. Samples doped with B and Sb compensating impurities ($N_D \approx 1.5 \times 10^{17}$, $N_A \approx 8 \times 10^{16}$) have also been studied. Again, it has not been possible to observe absorption due to excitons bound to ionized impurities.

---

1. E. J. Johnson and H. Y. Fan, Semiconductor Research, Signal Corps Contract DA 36-039-sc-87394, Final Report, October 1, 1961 to September 30, 1962.
2. M. D. Sturge, Phys. Rev. 127, 768 (1962).
3. Marshall I. Nathan and Gerald Burns, Phys. Rev. 129, 125 (1963).
4. Haynes, J. R., Phys. Rev. Letters 4, 361 (1960).

INFRARED ABSORPTION OF OXYGEN IN SILICON AND GERMANIUM UNDER HIGH RESOLUTION

A. K. Ramdas and R. L. Aggarwal

Oxygen enters into silicon crystals grown from silicon melted in quartz crucibles. An absorption band in such samples at around 9 microns has been correlated to dispersed oxygen in silicon by Kaiser, Keck, and Lange[1]. Hrostowski and Kaiser[2] established that it is due to the anti-symmetric mode of vibration of the bent Si-O-Si unit. An analogous band in germanium is observed[1] in germanium at 11.7 microns. At temperatures below $\sim 150^{\circ}K$ the 9 micron band in silicon exhibits a remarkable fine structure[2]. The object of the present investigation is to examine the fine structure for the above mentioned bands under high resolution as there is considerable interest regarding their origin[3].

Crucible grown samples of silicon with no intentional doping have been used. Oxygen was intentionally introduced in germanium via the ambient. A high resolution grating instrument equipped with blazed gratings was employed. The effective resolution under which the samples were measured was ~ 0.5 cm^{-1}. The absorption spectra were measured using a glass optical cryostat and liquid helium as coolant. The samples were cooled by conduction and the sample temperature is estimated to be $10\text{-}15^{\circ}K$.

Figure 23 shows the absorption spectra for silicon. Four absorption peaks have been clearly observed at 1128.1_9, 1132.7_0, 1134.5_1 and 1136.3_3 cm^{-1} respectively. Weak peaks have also been observed at 1124.7_5, 1126.5_1, and 1130.9_0 cm^{-1} respectively. The 1128.1_9 cm^{-1} peak shows a variation in strength from sample to sample. A number of other sharp but weak peaks have been observed in the range 1030-1120 cm^{-1} at 1084.9_2, 1099.3_0, 1103.9_6 and 1107.6_5 cm^{-1}. The origin of these bands is not yet clear.

According to Hrostowski and Alder[3] oxygen bonding the two nearest neighbour silicon atoms in the Si-O-Si unit, can tunnel from a potential minimum to any one of the other symmetrically equivalent minima, the symmetry resulting from the fact that the silicon atoms bonded to the oxygen atom are along < 111 > axis. The harmonic oscillator levels belonging to the anti-symmetric mode split as a result of the tunneling. The observed fine structure and its temperature variation can be qualitatively understood on this model. In the present work the fine structure has been observed with all its details clearly resolved and hence it will be possible to follow the temperature variation of the intensity of the components and deduce a model for the tunneling phenomenon. An optical cryostat with an exchange gas system has been set up for this purpose.

The anti-symmetric mode of vibration of Ge-O-Ge unit in germanium responsible for the 11.7 micron band also exhibits fine structure at low temperature and under high resolution (See Figure 24). The strongest peak at 862.20 cm^{-1} is followed by peaks at 862.8_5 and 863.8 cm^{-1} respectively. It is interesting to note that unlike in the case of silicon, the low frequency component is the strongest. A detailed examination of the fine structure is also planned as its origin appears to be similar to the analogous case of silicon discussed above.

It is known[4] that oxygen in silicon on heat treatment in the temperature range 300-600°C forms donor complexes. A series of absorption bands have been observed in a heat treated sample at 1043.8_7, 1052.0_6, 1057.6_0, 1059.7_7, and 1090.1_0 cm^{-1} and are presumably due to vibrations of various silicon oxygen complexes which behave like donors (See Figure 23). Some of these have been reported by Kaiser, Hrostowski, and Thurmond[5]. The donor complexes show electronic excitation spectra at low temperatures[6,7], and it appears that there are many species of such donors. It is of interest to correlate the vibrational absorption bands with the electronic excitation bands. Further work is in progress along these lines.

---

1. Kaiser, Keck and Lange, Phys. Rev. 101, 1264 (1946).

2. Hrostowski and Kaiser, Phys. Rev. 107, 966 (1957).

3. Hrostowski and Alder, J. Chem. Phys. 33, 980 (1960).
4. Kaiser, Frisch and Reiss, Phys. Rev. 112, 1546 (1958).
5. Kaiser, Hrostowski and Thurmond, Bull. Am. Phys. Soc., Ser. II, 5, 62 (1960).
6. Hrostowski and Kaiser, Phys. Rev. Letters, 1, 199 (1958).
7. Aggarwal and Ramdas, unpublished results.

II. IRRADIATION EFFECTS

ELECTRON PARAMAGNETIC RESONANCE IN SILICON AND GERMANIUM

G. S. Newell, W. Jung, D. Trueblood, and E. Hale

Introduction

In another report (hereafter referred to as "A")[1] we summarized the annealing curves and spin Hamiltonians of the paramagnetic defects which have been isolated during the annealing of pile-irradiated high resistivity silicon. We here discuss their hyperfine structures and also derive a better value for the absolute production rates. The material summarized in these two reports is discussed in detail in a thesis by W. Jung[2] and has been submitted for publication[3].

Helium temperature investigation of germanium irradiated with electrons at 77°K is in progress.

Hyperfine Structure

For Centers (II, III), (V, VI), and N, which were observed in large enough concentrations, the weak hyperfine satellites arising from the magnetic interaction of the electronic magnetic moments with neighboring Si^{29} nuclei ($I = \frac{1}{2}$, 4.7% abundant) were observed. The recorder trace of a Center (II, III spectrum ($H \parallel < 110 >$) which is reproduced in Fig. 20 shows these satellites. For Center (II, III), their amplitude ranges from 4 to 6% of satellites. For Center (II, III), their amplitude ranges from 4 to 6% of the main lines and is well above the noise level. The separation from the center line varies from 23 to 37 gauss and is fairly well resolved. For Centers (V, VI), and N, however, the hyperfine signals appear to be much weaker (only 2 to 3%) and are overshadowed by other centers at most angles, while the separation seems to be comparable to that of Center (II, III).

In addition, some of the well isolated branches of Centers (II, III), (V, VI), and (VII, VIII) show much more closely spaced satellites ("triplet structures") (Fig. 20) arising from hyperfine interactions with more distant nuclei. The lines on each side are separated from the center line by about 3 gauss and the amplitudes are 20 to 29% of the center lines.

The presence of several centers in each spectrum and an unfavorable signal to noise ratio prevented determination of the hyperfine tensor with any reliability except for Center (II, III). Even for Center (II, III) the "triplet" lines were so obscured by other branches that the hyperfine tensor for those satellites was not determined.

By including the hyperfine interaction term in the spin Hamiltonian, the hyperfine satellites are described by

$$\mathcal{H} = \beta \underset{\sim}{H}\cdot\underset{\sim}{g}\cdot\underset{\sim}{S} + \underset{\sim}{S}\cdot\underset{\sim}{\sigma}\cdot\underset{\sim}{S} + \underset{\sim}{I}\cdot\underset{\sim}{A}\cdot\underset{\sim}{S} + \beta_n g_n H\cdot I. \tag{1}$$

with $S = 1$.

Neglecting the last term, the first order energy shift due to one magnetic nucleus is

$$E(m_s m_I) - E(m_s, 0) = m_s m_I \left|\underset{\sim}{k}\cdot\underset{\sim}{A}\right| = m_s m_I A_e, \tag{2}$$

where $A_e^2 = \underset{\sim}{k}\cdot\underset{\sim}{A}^2\cdot\underset{\sim}{k}$; m_s, m_I are the electronic and nuclear magnetic quantum numbers; and $\underset{\sim}{k}$ is the unit vector in the direction of the effective field: $\underset{\sim}{k} = (g_e H)^{-1}\,\underset{\sim}{g}\cdot\underset{\sim}{H}$. As the microwave transitions correspond to $\Delta m_s = 1$, $\Delta m_I = 0$, the separation, ΔH, between the main and satellite lines is given by

$$g_e\beta\Delta H = m_I A_e \tag{3}$$

where $m_I = \pm\frac{1}{2}$ for Si^{29}. Hence the hyperfine interaction tensor, $\underset{\sim}{A}$, is determined from the angular variation of the quantity

$$A_e^2 = (2\, g_e\beta_0\Delta H)^2 \tag{4}$$

by applying the least squares procedure developed for the fine structure tensors.

The second order corrections to the hyperfine splittings are obtained from the Hamiltonian (Eq. 1) by a perturbation treatment in which $\vec{I}$ is kept in operator form[4]. The result is an effective nuclear Hamiltonian which for $I = \frac{1}{2}$ takes the form

$$\mathcal{H}_{\pm} = m\,\vec{k}\cdot\underset{\sim}{A}\cdot I + V_{|m|}\cdot I,$$

with

$$\vec{V}_{|m|} = \frac{1}{g_e\beta H}\left\{\left[3m^2 - S(S+1)\right]\left[\vec{k}\cdot\underset{\sim}{\sigma}\cdot\underset{\sim}{A} - (\vec{k}\cdot\underset{\sim}{\sigma}\cdot\vec{k})\,\vec{k}\cdot\underset{\sim}{A}\right] - \frac{1}{2}\left[S(S+1) - m^2\right](\mathrm{Det}\,\underset{\sim}{A})\,\vec{k}\cdot\underset{\sim}{A}^{-1}\right\} + g_n\beta_n\vec{H}$$

Here $g_e = |\vec{H} \cdot \underset{\sim}{g}|$ is the effective g value, $\underset{\sim}{g}$ is the zero field splitting tensor, and Det $\underset{\sim}{A}$ is the determinant of $\underset{\sim}{A}$. The last term is the direct interaction of the nucleus with the external field: it is a first order term, but has about the same magnitude as the second order corrections. The significant feature is that $\vec{V}_{|m|}$ is a vector which depends on $|m|$, not m, and hence aids the field seen by the nucleus in one $|m| = 1$ level and opposes it in the other. The corrected hyperfine splittings become:

$$\Delta H = \frac{1}{g_e \beta} \left[m_I A_e + \frac{m_s}{g_e \beta H} \left(\frac{\vec{k} \cdot \underset{\sim}{A} \cdot \vec{V}_1}{A_e} - |\vec{V}_o| \right) \right] ,$$

where $\vec{V}_1$, $\vec{V}_o$ are the values of $\vec{V}_{|m|}$ in the $m_s = \pm 1$, and $m_s = 0$ levels. For Center (II,III) at k-band the corrections are comparable to experimental error (~ 0.5 gauss) and are neglected. Under more favorable conditions, however, it may be possible to use the difference in the hyperfine splittings to assign absolute m_s values to the spectra.

The observed and calculated angular variation of the hyperfine splitting of Center (II, III) are plotted in Fig. 21. To measure a splitting, both the satellite and the main line must be visible; thus in constructing Fig. 21 points were taken from any of the 14 main branches which happened to be usable and are keyed to the corresponding branches plotted in Fig. 22 by using similarly coded lines. For Center (II, III), the following values are obtained:

$A_1 = (44.1 \pm 0.4) \times 10^{-4}$ cm^{-1} $\quad (\theta = 36.5^o \pm 0.5^o)$
$A_2 = (43.6 \pm 0.4) \times 10^{-4}$ cm^{-1}
$A_3 = (68.8 \pm 0.4) \times 10^{-4}$ cm^{-1}

where A_2 lies along $< 110 >$ and the axes are defined as usual[5]. These show a nearly axial $< 111 >$ symmetry; $A_\parallel = 68.8 \times 10^{-4}$ cm^{-1} and $A_\perp \approx \frac{1}{2}(A_1 + A_2) = 43.9 \times 10^{-4}$ cm^{-1} with $A_\parallel$ lying 1.2^o from $< 111 >$ toward $< 001 >$ in the (110) plane. In order to examine the overall fit of the parameters, the angular variations of the hyperfine satellite lines were calculated from the fitted values of $\underset{\sim}{g}$, $\underset{\sim}{\sigma}$, and $\underset{\sim}{A}$, and plotted for all of the 28 hyperfine branches corresponding to the 14 main lines. Figure 22 shows the actual angular variation plot for the unannealed Sample 2[6]. Exactly the same curves are obtained for Sample 4[6]. The thick lines represent the 14 main lines and the thin lines the corresponding hyperfine satellites, with both the parent and satellite lines coded in the same way as in Figs. 10 to 14 of (A). The fitted curves account for all of the visible portions of the hyperfine satellites remarkably well,

in fact within a line width. Further, all the lines visible at room temperature are accounted for. Those points in Fig. 22 which do not fall on the calculated curves belong either to the next nearest neighbor h f s. ("triplet structure"), or to Center IX.

The ratio of the amplitudes of the hyperfine satellites to the main lines was measured at those angles where both lines were well isolated from others. The observed ratio of 5.12% (σ = 0.78% from 32 measurements) is in satisfactory agreement with the value

$$[2I + 1]^{-1} \, [{}_2C_1 \, P(1-P)] \, / \, [{}_2C_0 \, (1-P)^2] \; = \; 0.0494$$

expected for two equivalent Si^{29} nuclei having $I = \frac{1}{2}$ and P = 0.047, and is easily distinguishable from the values of 2.47% expected for only one nucleus, 7.42% for three, and 9.89% for four.

For a spin I center such as Center (II, III), the orbitals localized on the two atoms overlap very slightly, giving rise to an exchange coupling. The observed hyperfine satellites correspond to the case in which only one of the two nuclei is Si^{29} ($I = \frac{1}{2}$), the other being Si^{28} ($I = 0$). Within the triplet manifold, the appropriate hyperfine Hamiltonian is

$$H_{hfs} \; = \; \tfrac{1}{2} \, \underset{\sim}{I}_1 \cdot \underset{\sim}{a}_1 \cdot \underset{\sim}{S}_1 \; + \; \tfrac{1}{2} \, \underset{\sim}{I}_1 \cdot \underset{\sim}{a}_1 \cdot \underset{\sim}{S}_2$$

$$\equiv \; \underset{\sim}{I}_1 \cdot \underset{\sim}{A}_1 \cdot \underset{\sim}{S}$$

where

$$\underset{\sim}{A}_i \; = \; \tfrac{1}{2} \, \underset{\sim}{a}_1 ; \quad i = 1 \text{ or } 2.$$

The hyperfine splitting of the energy level,

$$E(m_s, m_I) - E(m_s, 0) \; = \; m_s m_I \; \left| \, \underset{\sim}{k} \cdot \underset{\sim}{A}_1 \, \right| \; = \; \tfrac{1}{2} \, m_s m_I \; \left| \, \underset{\sim}{k} \cdot \underset{\sim}{a}_1 \, \right| ,$$

is exactly the same as for $S = \frac{1}{2}$, the value of $m_s = \pm 1$ canceling the factor of $\frac{1}{2}$. The fact that a <u>single</u> set of satellites of 5% relative amplitude is observed indicates that $\underset{\sim}{a}_1 = \underset{\sim}{a}_2$, and that the two nuclei are accurately equivalent. This suggests

that if the distortion of the hfs axis away from < 111 > is due to the mutual repulsion of the dangling bonds, these bonds are anti-parallel rather than parallel; in the latter case the hfs axis would differ by 2.4° and the nuclei would be clearly inequivalent.

Watkins and Corbett[7,8] discussed the hyperfine interaction of the electron irradiation centers in silicon (all $S = \frac{1}{2}$) on the following basis:

The wave function of the electron is approximated by 3s and 3p orbitals localized at various lattice sites j:

$$\psi = \Sigma_j \eta_j (\alpha_j \psi_{3s}{}^j + \beta_j \psi_{3p}{}^j),$$

where α_j and β_j are normalized according to $\alpha_j{}^2 + \beta_j{}^2 = 1$. The factor $\eta_j{}^2$ gives the fractional contribution from site j, and $\alpha_j{}^2$ and $\beta_j{}^2$ give the relative weights of 3s and 3p orbitals. The values of $\eta_j{}^2$, $\alpha_j{}^2$, and $\beta_j{}^2$ can be calculated from the observed A tensor:

$$a_j = \frac{1}{3}(A_{\parallel}{}^j + 2A_{\perp}{}^j) = \frac{16\pi}{3} g_N \beta_0 \beta_N \alpha_j{}^2 \eta_j{}^2 |\psi_{3s}(0)|^2,$$

$$b_j = \frac{1}{3}(a_{\parallel}{}^j - A_{\perp}{}^j) = \frac{4}{5} g_N \beta_0 \beta_N \beta_j{}^2 \eta_j{}^2 < r^{-3} >_{3p},$$

where g_N is the nuclear g factor, β_0 the Bohr magneton, and β_N the nuclear magneton. Using the value $|\psi_{3s}(0)|^2 / < r^{-3} >_{3p} = 1.4$ estimated from the tabulated Hartree functions and the value, $|\psi_{3s}(0)|^2 = 24 \times 10^{24}$ cm^{-3}, obtained from previous work on the Si-A center, the authors quoted obtain the values

$$a_j = \alpha_j{}^2 \eta_j{}^2 \times 1040 \times 10^{-4} \text{ cm}^{-1}$$

and

$$b_j = \beta_j{}^2 \eta_j{}^2 \times 36 \times 10^{-4} \text{ cm}^{-1}.$$

A similar analysis of the A tensor of Center (II,III) gives

$$a = 52.15 \times 10^{-4} \text{ cm}^{-1}, \quad b = 4.15 \times 10^{-4} \text{ cm}^{-1}$$

and hence $\alpha^2 = 0.176$, $\beta^2 = 0.824$, and $\eta^2 = 0.281$.

In terms of this simple model, the result is interpreted as follows: two orbitals of 18% 3s and 82% 3p character localized on two neighboring atoms account for 56% of the total wave function of each electron, the enhanced p-like character over the normal 25% 3s and 75% 3p (sp^3) tetrahedral orbital suggesting that the atom is pulled away from the normal site by its neighbors. The rest of the wave function is spread over more distant atoms.

The side lines of the "triplet" structure of Center (II, III) may account for a large portion of the remaining wave function. The relative amplitude varies from 20 to 29% (23.6%, σ = 3.7% from 30 measurements), and it is difficult to distinguish among the values of 19.8% expected for eight equivalent nuclei, 24.7% for ten, and 29.7% for twelve. As the approximately ten neighboring atoms are almost certainly not equivalent for arbitrary orientations of the magnetic field, these satellites should split into groups characteristic of the structure of the center. Unfortunately, the resolution is such that the lines merely broaden and disappear. The fact they are visible over quite a range of angles reflects the small value of the coupling constant for 3p states.

Obscuration of the lines and inadequate resolution thus prevent determination of the hyperfine tensor for these atoms and only rather broad limits can be placed on their contribution to the total wave function. The separations from the center lines are about 3.1 gauss and are nearly constant over the region where they are visible. The separation corresponds to 5.8×10^{-4} cm^{-1}. Assuming $A \approx 5.8 \times 10^{-4}$ cm^{-1} as a reasonable guess, and assuming little disturbed normal sp^3 orbitals ($\alpha^2 = 0.25$ and $\beta^2 = 0.75$), $A_{||} = 1.35\ A_{\perp}$ and hence $\eta^2 \sim 0.026$. Thus by taking ten nuclei, the contribution to the total wave function amounts to 26%. However, the data are insensitive to the p component. Taking $a^2 = 1$ as the extreme case, $\eta^2 = .006$ and the contribution to the wave function would be only 6%

The interpretation that the triplet structures arise from the interaction with a number of distant nuclei is confirmed by the occasional detection of a second pair of very faint satellites having the separations and amplitudes predicted for interactions involving <u>two</u> Si^{29} nuclei among the 8 to 12 neighbors.

The spectra of both main and hyperfine satellite lines, and their relative intensities, remain unchanged between 300°K and 77°K. This suggests that the electronic configuration is rather firmly locked and not affected in this temperature range.

In contrast, the spectrum of the N Center goes through a transition at temperatures between 77°K and 166°K. While the hyperfine tensor at 300°K cannot be determined accurately because of an unfavorable signal to noise ratio, the hyperfine

splitting is only one-half that of the 77°K spectra, and the relative amplitude of the satellites remains unchanged at about 2%. This suggests that at 300°K, the electronic wave function is distributed by a motional effect over two atoms which are not quite equivalent. The hyperfine interactions involving two similar but not equivalent sites should give rise to twice as many satellite lines as for two equivalent sites, each having 2.5% amplitude and comparable separations, and would make the experimental determination of the tensors much more difficult. This may very well be the case of Center (V, VI) also; in fact, the anisotropy of the g tensor of the center is consistent with a pair of two $< 111 >$ dangling bond orbitals oriented toward the center of a tetrahedron and thus supports the suggestion.

In summary, the h.f.s. data unequivocally confirm the model for Center (II, III) consisting of two electrons localized in parallel (or, more likely, antiparallel) dangling sp^3 orbitals centered on different atoms. It is tempting to suppose that Center (II, III) represents the neutral state of the divacancy, as is suggested by the number of next nearest neighbors, but this assignment is incompatible with the work of Watkins and Corbett on the Si-C and Si-J centers on the ground that Center (II, III) anneals at too low a temperature and fails to show re-orientation near 77°K.

The higher temperature S = 1 centers are probably similar to Center (II, III) but with the addition of oxygen bridges.

Defect Concentrations:

Figures 8 and 9 of (A) plot the amplitude of the fine structure lines of the various centers relative to 100 for the internal ruby standard. Our original derivation[9] of absolute defect concentrations from these curves of necessity omitted corrections for the hyperfine intensities, and in addition, contained an error of a factor of 4 in the transition matrix element for ruby. A corrected treatment follows:

From the amplitude of a center relative to that of the internal ruby standard, its absolute concentration can be estimated using the relation

$$n_s = \frac{N_s}{V_s} = N_r \frac{\eta_r \alpha_r C_s A_s (\Delta H_s)^2}{\eta_s \alpha_s C_r A_r (\Delta H_r)^2} \frac{12}{V_s}$$

$$= 5.25 \times 10^{15} \frac{(\Delta H_s)^2}{\alpha_s} \frac{A_s}{A_r},$$

where the symbols are defined as follows:

$\frac{\eta_r}{\eta_s} = \frac{Hrf^2 \text{ ruby}}{Hrf^2 \text{ sample}}$ = the relative filling factor = 0.216.

α_s = transition probability factor = $\frac{S(S+1)-m_s(m_s+1)}{2S+1}$.

α_r = 1.02 instead of 1 for the $m_s = -\frac{1}{2}$ to $+\frac{1}{2}$ transition of Cr^{+3} in ruby due to the matrix element correction.

ΔH_s = line width
ΔH_r = line width of ruby signal = 15.9 gauss. (Full width between inflections).
N_r = number of Cr^{+3} spins in 1.79 mg of ruby $\approx 2.07 \times 10^{16}$.
V_s = sample volume = $1.03 \times .43 \times .093 = 4.12 \times 10^{-2}$ cm^3.
A_s/A_r = amplitude ratio
C_s, C_r = line shape factors: $C_s = C_r$, assuming the same line shape (gaussian).

The factor of 12 results from the fact that the amplitudes plotted in Fig. 5 are for a single branch normalized to unit multiplicity.

The peak concentrations of the centers at various stages of annealing are collected in Table II. The table includes corrections for (1) hyperfine satellite lines and for (2) singlet level populations for the spin 1 centers. For Center (II, III), for example, weak satellites (4.9%) and the "triplet" satellites (23.6%) give rise to ~ 57% hfs correction. For Centers (V, VI) and (VII, VIII), only the "triplet" satellites are taken into account and hence the 50% correction is only approximate. For the N center, no "triplet" structure was observed and the correction represents the contribution of the weak satellites alone. The singlet level population corrections for spin 1 centers were assumed to be $+\frac{1}{3}$ by taking a statistical weight of 1/4 for the singlet levels and neglecting the Boltzmann factor.

The value of 2.07×10^{17} spins in the ruby standard is calculated from the nominal concentration of 0.1% Cr^{+++}. Although it is certainly in error, it is being used until we are better satisfied with the accuracy of our own determinations. These have been: (1) comparison of the resonance amplitude with that of a known sample of $Cu\,SO_4 \cdot 5\,H_2O$, giving 1.2×10^{16} spins for the ruby, and (2), a measurement of the optical density at selected wavelengths[10], giving 1.4×10^{16} spins:

Erratum:

In (A), p. 15, the equation relating the observed fields for resonance to the values of g and σ read from the calculated curves should read.

TABLE II

Peak Concentrations of EPR Centers in Neutron Irradiated Silicon

Sample 2 (USSC #4, $\phi = 1.4 \times 10^{18}$ nvt, ORNL)

Centers	S	Δ H (gauss)	A/Ar	n (10^{15} cm^{-3})	Corrections hfs	Corrections singlet	Final (10^{16} cm^{-3})	Impurity dependence
(II, III)	1	1.2	.359	4.07	+ 57%	+ 33.3%	.85	Independent
IX	$\frac{1}{2}$	1.4	.155	3.19	unknown	--	.32	Independent
N	$\frac{1}{2}$	1.2	.451	6.82	+ 9.8%	--	.75	Independent
(I, I')	1	2.4	.0576	2.59	unknown	+ 33.3%	.35	Oxygen dependent
(V, VI)	1	1.2	.442	5.02	+ 50%	+ 33.3%	1.00	Oxygen dependent
(VII, VIII)	1	1.6	.0478	0.97	+ 50%	+ 33.3%	.19	Oxygen dependent

$$H = \frac{h}{\beta_o} \frac{\nu \pm \frac{3}{2}\sigma}{g} .$$

Taking the average elastic scattering cross section of silicon atoms for fast neutrons to be ≈ 3 barns, the number of collisions is 2.1×10^{17} per cm^3 for a flux of 1.4×10^{18} nvt, giving peak production rates of 0.01 to 0.05 centers per collision. In view of the large number of knock-ons (≈ 20) expected, this small value appears significant.

---

1. Semiconductor Research, Contract DA 36-039-sc-87394, Eighth Quarterly and Final Report, October 1, 1961 - Sept. 30, 1962.
2. W. Jung, Thesis, Purdue University, 1963.
3. W. Jung and G. S. Newell, Phys. Rev. (to be published).
4. The derivation is somewhat lengthy. (See reference (1).
5. A_2 is along $< 110 >$, A_1 lies in the plane containing $< 001 >$ and $< \bar{1}10 >$, making an angle θ with $< 001 >$, and A_3 lies in the same plane, perpendicular to A_1.
6. Sample 2 = crucible grown; Sample 4 = floating zone. See table II of (A) for details.
7. G. D. Watkins and J. W. Corbett, Phys. Rev. 121, 1001 (1961).
8. G. D. Watkins and J. W. Corbett, Discussions Faraday Soc. 31, 89 (1961).
9. Semiconductor Research; Contract DA 36-039-sc-87394, Fifth Quarterly Report, October 1, 1961 - December 31, 1961, p. 12.
10. The absolute absorption coefficient of ruby vs. wavelength is given by T. H. Maiman et al, Phys. Rev. 123, 1151 (1963).
11. D. J. Hughes and J. A. Harvey, Neutron Cross Sections, BNL 325, Brookhaven National Laboratory, 1955. The total cross section, σ_T, varies from 2 to 4 barns for 0.1 to 10 MeV neutrons.

III. LOW TEMPERATURE STUDIES

SPECIFIC HEAT OF LEAD BETWEEN 0.3 AND 4°K

P. H. Keesom and B. J. C. van der Hoeven, Jr.

It is found that C_{es}, the electronic contribution to the specific heat of superconductive lead, below 1°K, exceeds the value calculated by the BCS[1] theory by several orders of magnitude. Instead, C_{es} shows reasonable agreement with a T^3 dependence for values of $t = T_c/T$ between 2 and 22.

A lead sample of 1.293 moles (99.999% purity) was measured and the results in the normal and superconductive states can be represented by

$$C_n = 2.98\ T + 1.60\ T^3 + 0.028\ T^5 \text{ mJ/mole deg}, \quad (1)$$

$$C_s = 0.144\ T^3 + 1.60\ T^3 + 0.028\ T^5 \text{ mJ/mole deg}. \quad (2)$$

The accuracy above 1°K is 1 - 2%, and 2 - 3% below this temperature.

The last two terms in both equations originate from the lattice vibrations and give for the Debye parameter at 0°K: $\theta = 106.7 \pm 0.5$°K. This is in good agreement with results calculated from velocity of sound measurements (105°K)[2]. The linear term in eq. (1) arises from the electronic contribution. This agrees with the value for the coefficient of 3.06 ± 0.04, deduced from critical field measurements by Decker, et al.[3], within the combined limits of accuracy.

The electronic contribution in the superconductive state, C_{es}, is calculated in the BCS theory to be:

$$C_{es}/\gamma\ T_c = 8.5 \exp(-1.44\ T_c/T). \quad (3)$$

Decker et al. already noticed deviations from this equation in their critical field measurements up to $t = 6$. If the first term in eq. (2) is identified with C_{es}, it follows that eq. (3) is inadequate to represent the data, as can be seen in fig. 1. In this graph is plotted in $(C_{es}/\gamma\ T_c)$ versus T_c/T. In the same graph the function $0.144\ T^3/\gamma\ T_c$ is also drawn, which represents the data within the accuracy for this term (10 - 20%).

Cooper[4] proposed that anisotropy in the energy gap would lead to two exponential temperature dependences for C_{es}. However, the result of our measurements is very different from that expressed in eq. (3). It does not appear possible to represent the data with two exponentials, within reasonable limits for anisotropy.

Ginsberg et al.[5] observed, in lead, precursors in the absorption of electromagnetic waves with energies about $\frac{1}{5}$th of the energy gap. One could assume a narrow set of energy levels in the energy gap, but for such a set to lead to a T^3 contribution in the specific heat appears rather unlikely.

A curious result can be obtained in the following way. A T^3-dependence for C_{es} leads thermodynamically to the parabolic law for the critical field:

$$H = H_o(1 - (T/T_c)^2) \ . \qquad (4)$$

Using the relation between ΔC($\Delta C = C_s - C_n = 0.144\ T^3 - 2.98\ T$) and d^2H^2/dT^2 we find $H_o = 806$ Gauss, in excellent agreement with the value found from magnetic data ($H_o = 802.6$ Gauss). However, this analysis also yields a value of $T_c = 7.88^oK$, whereas the normal transition temperature for lead is 7.19^oK. Eq. (4) agrees reasonably well with magnetic measurements below 2^oK, but above this temperature it leads to ever increasing discrepancies. Therefore, the specific heat should contain other terms than the T^3 one which appear, however, to be small. If one lets T_c in eq. (4) be temperature dependent,

$$T_c = 7.88 - \ln (1 + T/7.19) \ , \qquad (5)$$

the magnetic data below 7^oK are represented within 1 Gauss. This formula cannot be correct, for it predicts a negative T^2 term in the specific heat, which is not observed below 1^oK. Still the success of this temperature dependence of T_c, to which the energy gap is related, suggests two possibilities:

1. The lowering of the energy by pairing the electrons is temperature dependent or
2. The temperature dependence of the energy gap is stronger for lead than that calculated by the BCS theory.

Later measurements of a single crystal sample of lead gave values for the specific heat in the normal and superconducting state of:

$$C_n = 3.03\ T + 1.61\ T^3 + 0.023\ T^5$$

$$C_s = 0.144\ T^3 + 1.61\ T^3 + 0.028\ T^5$$

---

1. J. Bardeen, L. N. Cooper and J. R. Schrieffer, Phys. Rev. 108 (1957) 1175.
2. D. L. Waldorf and G. A. Alers, J. Appl. Phys. 33 (1962) 3266.

3. D. L. Decker, D. E. Mapother and R. W. Shaw, Phys. Rev. 112 (1958) 1888.
4. L. N. Cooper, Phys. Rev. Letters 3 (1959) 17.
5. D. M. Ginsberg, P. L. Richards and M. Tinkham, Phys. Rev. Letters 3 (1959) 337.

THERMAL CONDUCTIVITY AND THERMOELECTRIC POWER

N. Pearlman

The large increase in thermal resistance which has been observed at low temperatures in Ge doped with Sb and As and its diminution on compensation with Ga has been shown in previous Progress Reports to depend on the concentration of neutral donors, N_d^o in the material. The effect is larger for Sb donors than for As in concentration ranges where the impurity levels are in the energy gap and not in the conduction band. Recently, Carruthers and Griffin[1] have proposed a mechanism for this effect which differs in some respects from that proposed earlier by Keyes, although the results of their calculations are in general agreement with those of Keyes and with the measurements. Their calculations contain predictions which are of interest with regard to the projected extension of our measurements below 1^oK and also with respect to the conclusions that can be drawn as to the nature of the electron levels in compensated material with large impurity concentrations.

Keyes calculated the scattering of phonons as a result of the virtual transitions between the singlet ground state and the triplet excited state, higher by 4Δ, in the neutral donor atoms, using the elastic strain due to the phonons as the perturbation responsible for the transitions. The coupling constant for static strains is related to 4Δ, and the difference in this quantity between Sb and As accounted for the observed difference in the magnitude of added thermal resistance for the two impurities. Carruthers and Griffin object to this procedure on the ground that it is applicable to the dynamic phonon strain only for phonon frequency ω much less than $4\Delta/\hbar$, whereas the effect occurs at temperatures for which the dominant phonons have $\omega \approx 4\Delta/\hbar$. They therefore calculate the cross-section for resonance fluorescent scattering of phonons, involving the triplet and singlet levels. When they take boundary scattering into account as well they find excellent agreement with the measured values between 4^oK and 1^oK, including the difference observed in temperature dependence of thermal conductivity (T^4 for Sb; T^3 for As).

At higher temperatures the calculations give values of thermal conductivity which are too high, presumably because of the neglect of Umklapp scattering. Below 1°K they predict a rather sharp decrease in the extra resistance, which should be easily observed within the planned precision of our projected measurements.

Although Carruthers and Griffin confine themselves to the non-compensated case, their calculation does contain information about compensated material as well. It is based on the wave-function of the bound donor electron, and in particular the amplitude at small distance from the core determines the cut-off in the extra thermal resistance at higher phonon frequencies, that is, at higher temperatures. Now the effect in compensated material has been shown to be the same as that in non-compensated material with the same concentration N_d^o, even though the total impurity concentration N_I is 100 times larger in the compensated case. This means that the wave-function does not differ enough in the two cases to make a difference in the calculation of thermal resistance. We have previously presented evidence from electrical resistance and Hall effect measurements that whereas the donor levels overlap the conduction band for sufficiently high N_I in single-doped Ge they must be in the energy gap in compensated material with comparable N_I but much lower N_d^o. The calculations of Carruthers and Griffin present the possibility that this earlier qualitative conclusion may lead to a quantitative upper limit on the permissible difference between the compensated Ge with comparable concentrations N_d^o.

IV. GENERAL

X-RAY LATTICE PARAMETER

R. C. Buschert

Preliminary measurements, to test the equipment and the method, on the change in lattice parameter of germanium due to doping with arsenic have been made. In the method used, the change in lattice parameter of the single crystal being measured is determined by measuring the angular shift in a diffraction line position (12, 0, 0) between the sample and a standard undoped single dislocation free germanium crystal. The first sample was arsenic doped to $\sim 10^{19}$/cc and showed an angular line shift of 20" of arc. This indicates a lattice parameter increase of $\Delta\, d/d = + 5 \times 10^{-5}$.

The half width of the diffraction line increases from 0.6" of arc for the undoped dislocation free reference crystal to 30" of arc for the arsenic doped crystal (with many dislocations). It is presumed that most of this broadening is due to dislocations. However the possibility exists that the lattice parameter change may be partly due to the dislocations. At the present an undoped sample with dislocations is being prepared in order to determine the influence of dislocations on the lattice parameter.

In order to accurately determine the concentration of the impurities gallium and arsenic in germanium work has been done on neutron activation of these elements in the Purdue nuclear reactor.

This bombardment and activity measurement indicated that it should be possible to determine the concentration of either or both (as in a compensated sample) of these impurities in germanium to a precision of (1 - 5)% for concentrations of 10^{17}/cc and greater.

GROWTH OF SINGLE CRYSTALS OF ZINC TELLURIDE

P. Klose and H. Y. Fan

Single Crystals of Zinc Telluride have been grown from the vapor phase and by the Bridgman technique. Both methods have been used with equal results. Since the Bridgman technique permits higher growth rates than the vapor phase method, most crystals have been grown in this fashion.

The crystals have been checked with x-rays and optical methods to determine the orientation and size of the individual grains of an ingot. Usually from two to four grains made up an ingot of about three cm^3. Experimental specimens have been cut so as to avoid grain boundaries.

A mullite pressure container was used to contain the vacuum sealed quartz ampoule which served as crucible. This container became especially useful during the doping experiments with arsenic, indium, and gallium where vapor pressures of several atmospheres had to be sustained by the quartz ampoule.

Measurements of Hall coefficient and resistivity have been made on several samples in the temperature range from $300^{o}K$ to $78^{o}K$. The results are tabulated below. Figures (26) and (27) show the temperature dependence of the Hall coefficient and the resistivity of Zinc Telluride samples doped with various concentrations of arsenic ranging from $2.6 \times 10^{16}/cm^3$ to $1.6 \times 10^{18}/cm^3$. The activation energy as calculated from the Hall data varies in that range from zero to 0.098 eV. Most of the samples grown without doping show activation energies around 0.15 eV. The activation energy of copper impurity has been reported by M. Aven to be 0.15 eV.

Doping with gallium did not change the type of the usually p-type crystals but changed the Hall coefficient from 10^2 cm^3/coul to 10^5 cm^3/coul. Doping with indium produced n-type material with a Hall coefficient of 10^6 cm^3/coul. So far we have not successfully grown n-type crystals of higher carrier concentration. Attempts are still being made.

Samples	300°K		78°K		Remarks
	R $\frac{cm^3}{coul}$	ρ (Ω-cm)	R $\frac{cm^3}{coul}$	ρ (Ω-cm)	
ZnTe - 37	+ 100	1.2	+ 6.9×10^5	1.6×10^5	Vapor phase-As
ZnTe - 38	+ 425	4.94			Vapor phase
ZnTe - 59	+ 77.5	0.67	+ 1.9×10^8	7.4×10^4	Bridgman
ZnTe - 111	+ 285	2.5			Bridgman
ZnTe - 125	+ 217	2.5	+ 1.2×10^9		Bridgman
ZnTe - 133	+ 84.4	1.0	+ 3.6×10^7	9.2×10^4	Bridgman
ZnTe - 141	+ 1140	24.1			Bridgman
ZnTe - 145	+ 40.8	0.51	+ 2.6×10^4	65.3	Bridgman-As
ZnTe - 146	+ 196	1.54			Vapor phase
ZnTe - 147	+ 2.93×10^5	6.2×10^4			Bridgman-Ga
ZnTe - 150	- 1.3×10^6	2.48×10^4			Bridgman-In
ZnTe - 151	- 2.9×10^6	3.86×10^4			Bridgman-In
ZnTe - 152	+ 244	2.68	+ 5.3×10^8		Bridgman-As
ZnTe - 154	+ 4.1	0.16	+ 3.3	0.47	Bridgman-As
ZnTe - 155	+ 55.5	0.66	+ 2.64×10^5	8.95×10^3	Bridgman-As

PUBLICATIONS

B. J. C. van der Hoeven, Jr. and P. H. Keesom, "Specific Heat of Lead between 0.3° and 4°K", Physics Letters 3, 360 (1963).

G. Sadasiv, "Magnetoresistance in Germanium in the Impurity Conduction Range", Phys. Rev. 128, 1131-1135 (1963).

E. J. Johnson, I. Filinski and H. Y. Fan, "Absorption and Emission of Excitons and Impurities in GaSb." Proceedings of the International Conference on the Physics of Semiconductors, Exeter (1962).

R. J. Sladek, "Piezothermal Conductivity of Doped Ge." Ibid.

R. Bray (with J. Appel and E. G. Wigner), "Electron-Electron Scattering in Semiconductors: Theory and Experiment." Ibid.

H. Y. Fan (with A. F. Kravchenko), "Galvano- and Thermomagnetic Effects in N-type GaAs." Ibid.

MEETINGS ATTENDED AND PAPERS PRESENTED

Tenth Annual Midwest Solid State Conference, Kansas City, Mo., October 1962.
W. M. Becker, "Galvanomagnetic Effects in N-type GaSb."

Conference on Superconductive Magnets, Boston, Mass., December 1962.
P. H. Keesom attended.

American Physical Society, New York, January 1963.
B. J. C. van der Hoeven, Jr., "Low Temperature Specific Heat of Various Graphites between 0.4 and 2.0°K."

American Physical Society, St. Louis, Mo., March 1963.

R. J. Sladek, "Piezoresistance of n-type GaAs."

V. A. Johnson (with P. Skadron), "Effect of Annealing on the Electrical Properties of Single Crystal Te."

P. H. Keesom and B. J. C. van der Hoeven, Jr., "Specific Heat of Pb between 0.3° and 4°K."

W. M. Becker and H. Y. Fan, "Oscillatory Magnetoresistance of GaSb."

Wun Jung and G. S. Newell, "Spin 1 Centers in Neutron-Irradiated Si."

W. Pinson and R. Bray, "Experimental Determination of Hot Carrier Distribution Function in P-type Ge," and "Hot-carrier Analysis with Experimental Distribution Functions."

CAPTIONS FOR FIGURES 20-22

Fig. 20. EPR spectrum of Center (II, III) with H $\|$ < 110 >. Sample 4 (Vacuum Floating zone silicon, $\phi = 1.8 \times 10^{18}$ nvt at ORNL) annealed at 100°C for 30 minutes. T = 300°K, ν = 24.552 108 kMc. The principal lines are marked according to whether they belong to Set II or Set III. The hyperfine satellites (5.1% relative amplitudes) due to the Si^{29} nuclei in the nearest lattice sites and the "triplet" structure (23.6% relative amplitudes) due to those in next nearest sites are visible on one of the isolated branches.

Fig. 21. Hyperfine splitting of Center (II, III). The separation between the hfs satellites (5.1% relative amplitude) and the corresponding branches of the fine structure is plotted vs the orientation of the external field in a (110) plane. Points taken from the $m_s = 0$ to ± 1 transitions fall on the same curves and are not distinguished.

Fig. 22. Angular variation plot of Center (II, III) spectrum. Sample 2 (Crucible grown silicon, $\phi = 1.4 \times 10^{18}$ nvt at ORNL), unannealed. T = 300°K, ν = 24.112 101 kMc. The external magnetic field, shown in proton resonance frequency (Mc), is rotated in a (110) plane. The open circles belong to Set II and the closed circles to Set III. The diameter of the circles corresponds to the full width between inflections of the resonance lines. The thick lines represent the fine structure lines and the thin lines the hyperfine satellite lines. The branches are coded by solid, dashed, and dotted lines to indicate the pairs belonging to the same orientation of the center. The "triplet" lines are also shown on two upper branches of Set II.

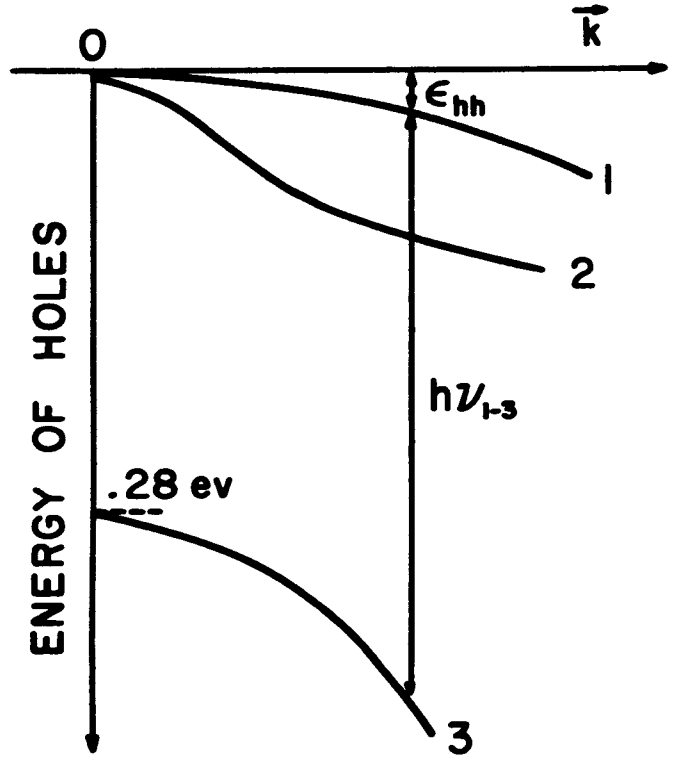

GERMANIUM VALENCE BANDS

INTERBAND FREE CARRIER ABSORPTION

$$\alpha_{13}(\lambda_i) \sim \frac{p(\epsilon_{hh})H_{13}^2}{h\nu\, f(m_1^*, m_3^*)} \qquad (1)$$

ASSUMPTION

$\alpha(\lambda_i) = C \cdot p(\epsilon_{hh})$ only (2)

C INDEPENDENT OF

$T_{CRYSTAL}$ or $\vec{E}$

FIGURE 1

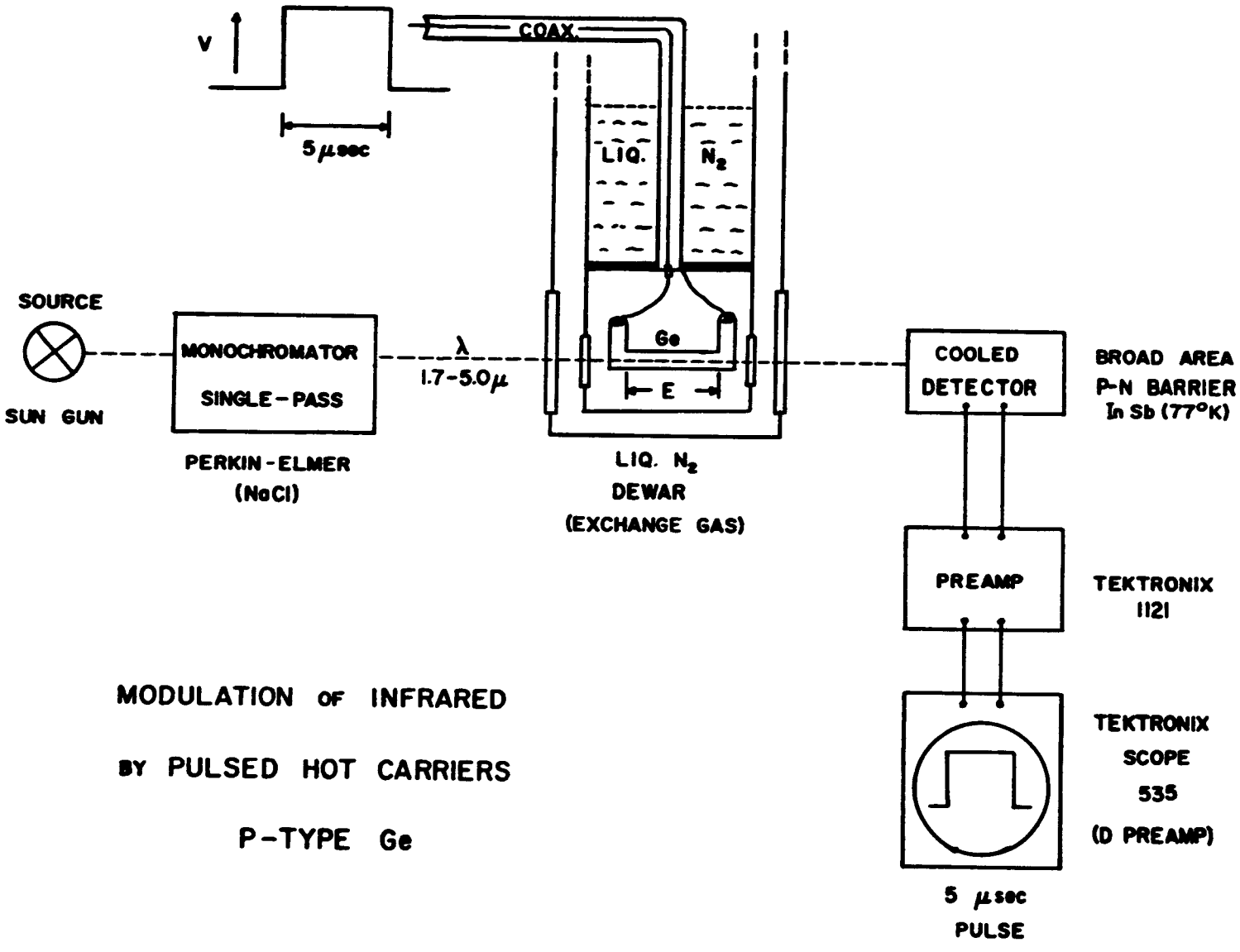
V
5 μsec
COAX.
LIQ.
N2
SOURCE
SUN GUN
MONOCHROMATOR
SINGLE-PASS
PERKIN-ELMER
(NaCl)
λ
1.7-5.0μ
Ge
E
LIQ. N2
DEWAR
(EXCHANGE GAS)
COOLED
DETECTOR
BROAD AREA
P-N BARRIER
In Sb (77°K)
PREAMP
TEKTRONIX
1121
TEKTRONIX
SCOPE
535
(D PREAMP)
5 μsec
PULSE
MODULATION OF INFRARED
BY PULSED HOT CARRIERS
P-TYPE Ge

FIGURE 2

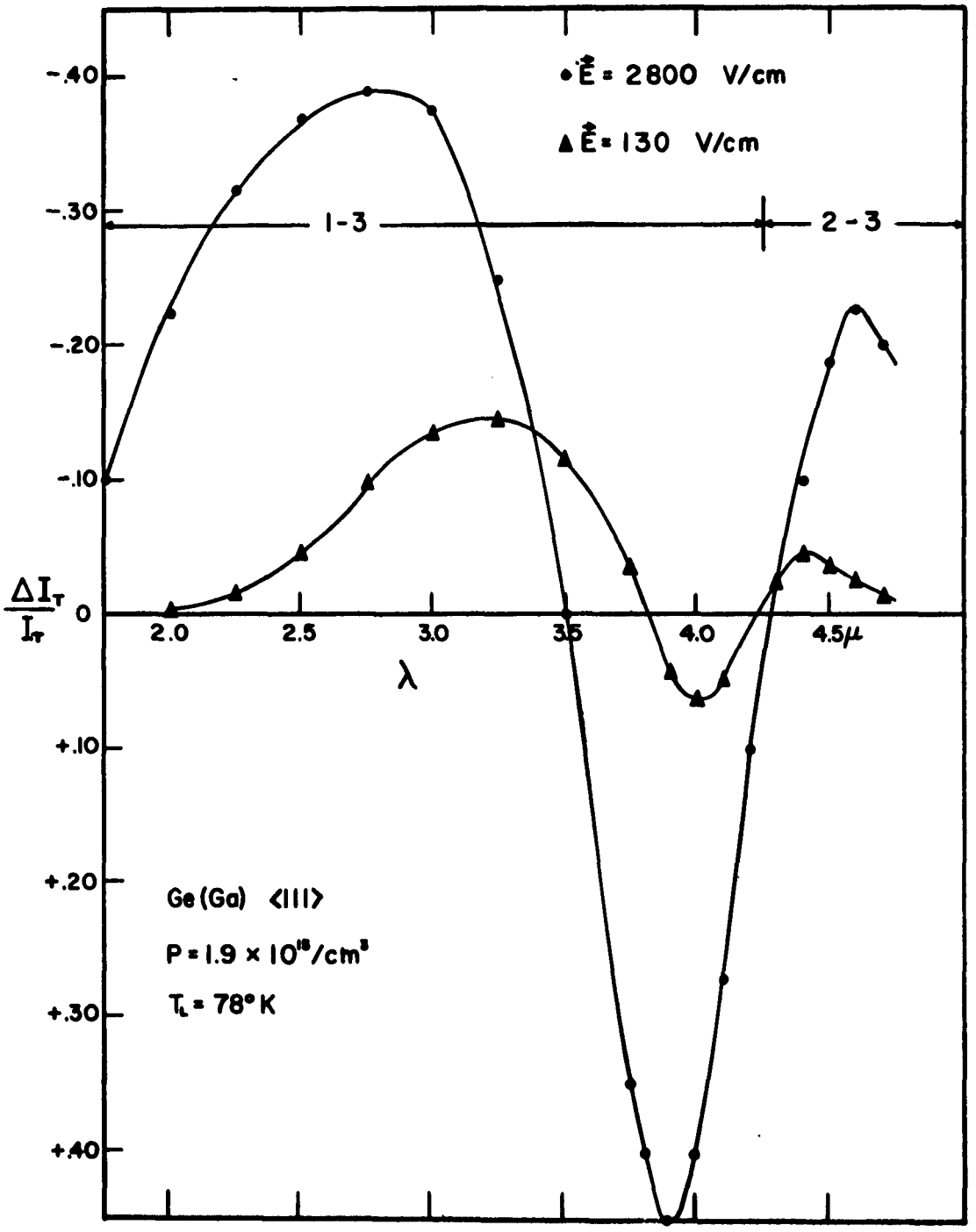
-.40
-.30
-.20
-.10
0
+.10
+.20
+.30
+.40
$\frac{\Delta I_T}{I_T}$
2.0
2.5
3.0
3.5
4.0
4.5μ
λ
• $\hat{E}$ = 2800 V/cm
▲ $\hat{E}$ = 130 V/cm
1-3
2-3
Ge (Ga) ⟨111⟩
P = 1.9 × 10¹⁸/cm³
T_L = 78° K

FIGURE 3

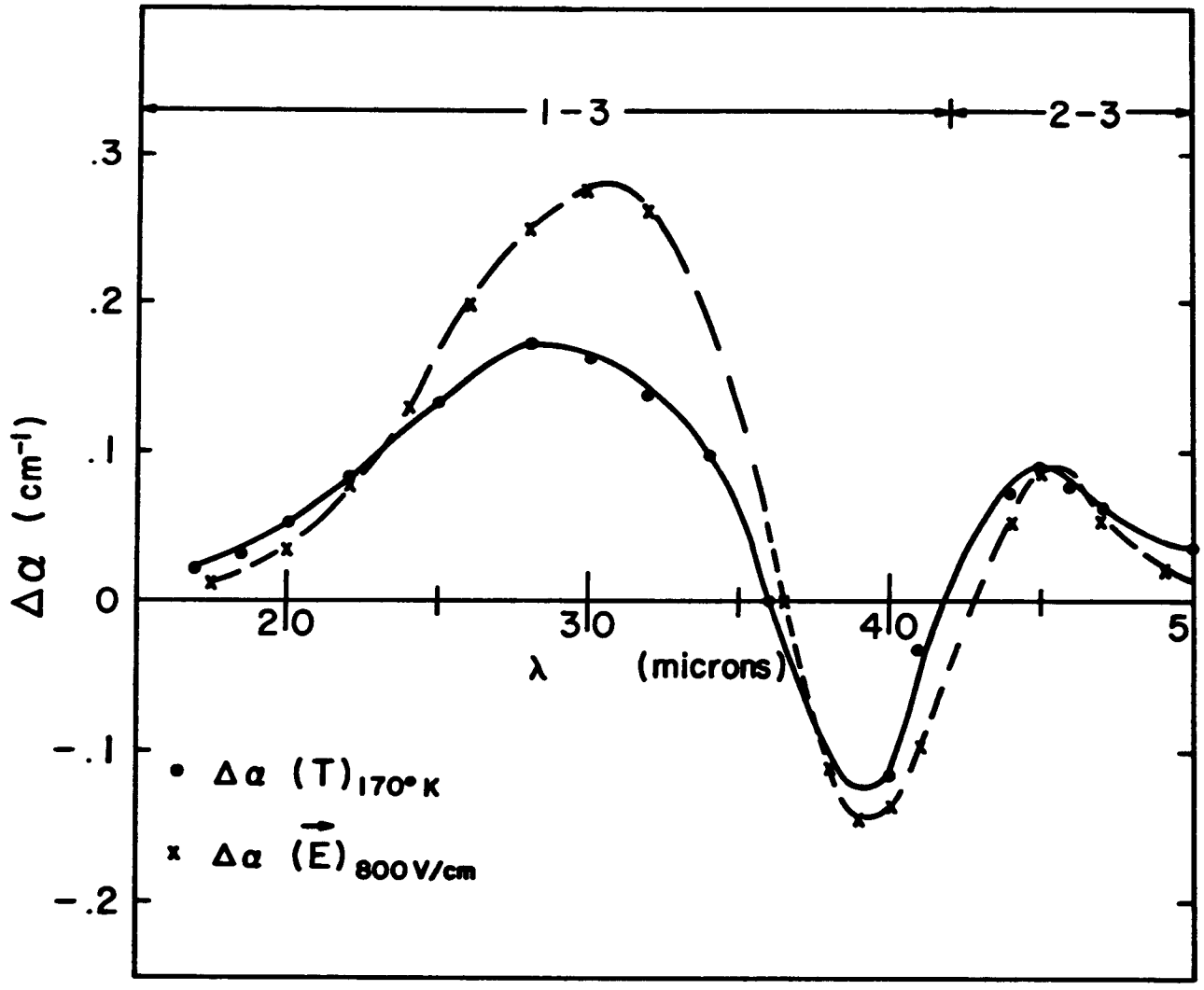

FIGURE 4

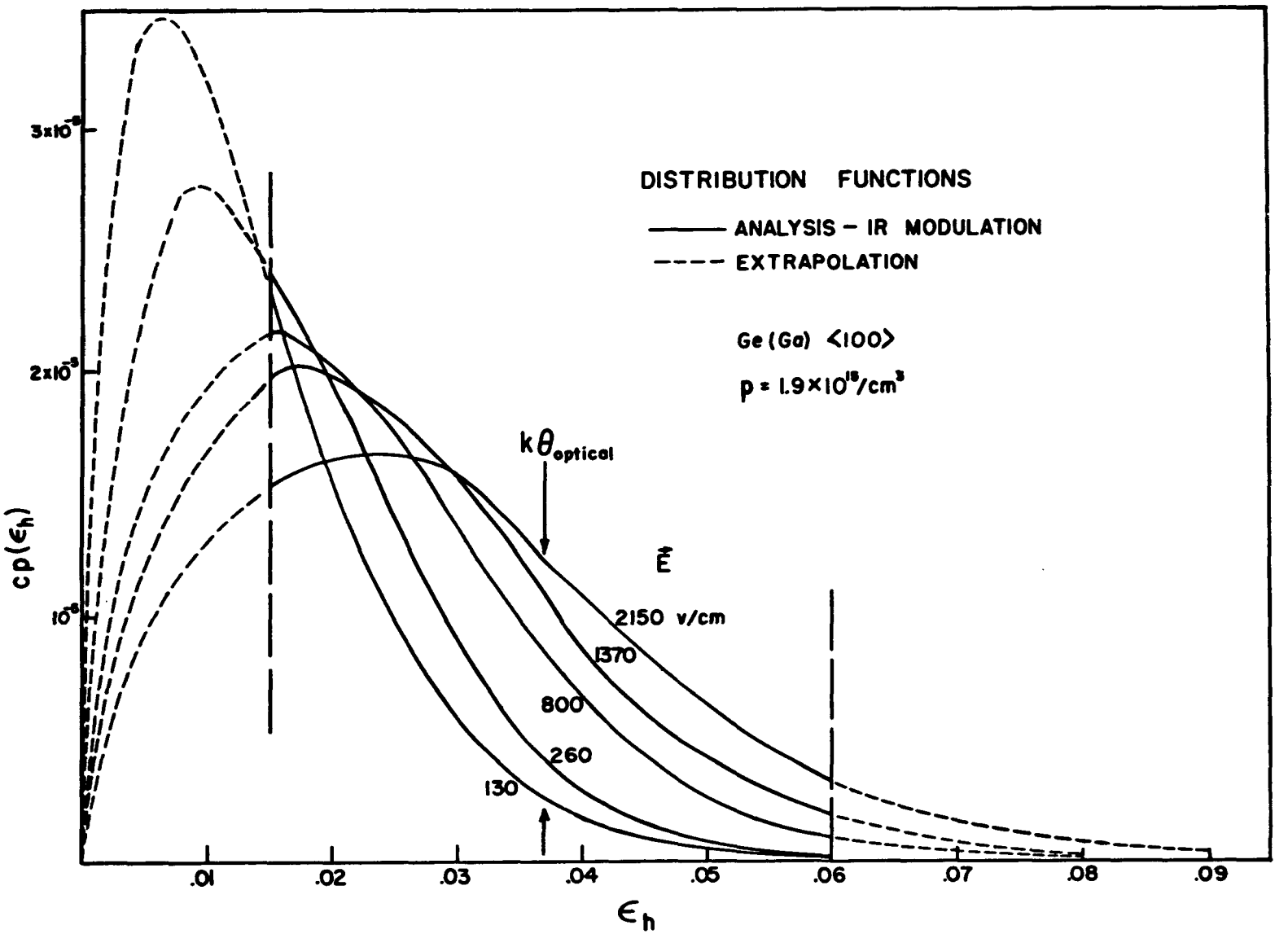
DISTRIBUTION FUNCTIONS
ANALYSIS – IR MODULATION
EXTRAPOLATION
Ge (Ga) <100>
p = 1.9×10^18/cm^3
kθ optical
Ē
2150 v/cm
1370
800
260
130
cp(ε_h)
ε_h
.01
.02
.03
.04
.05
.06
.07
.08
.09

FIGURE 5

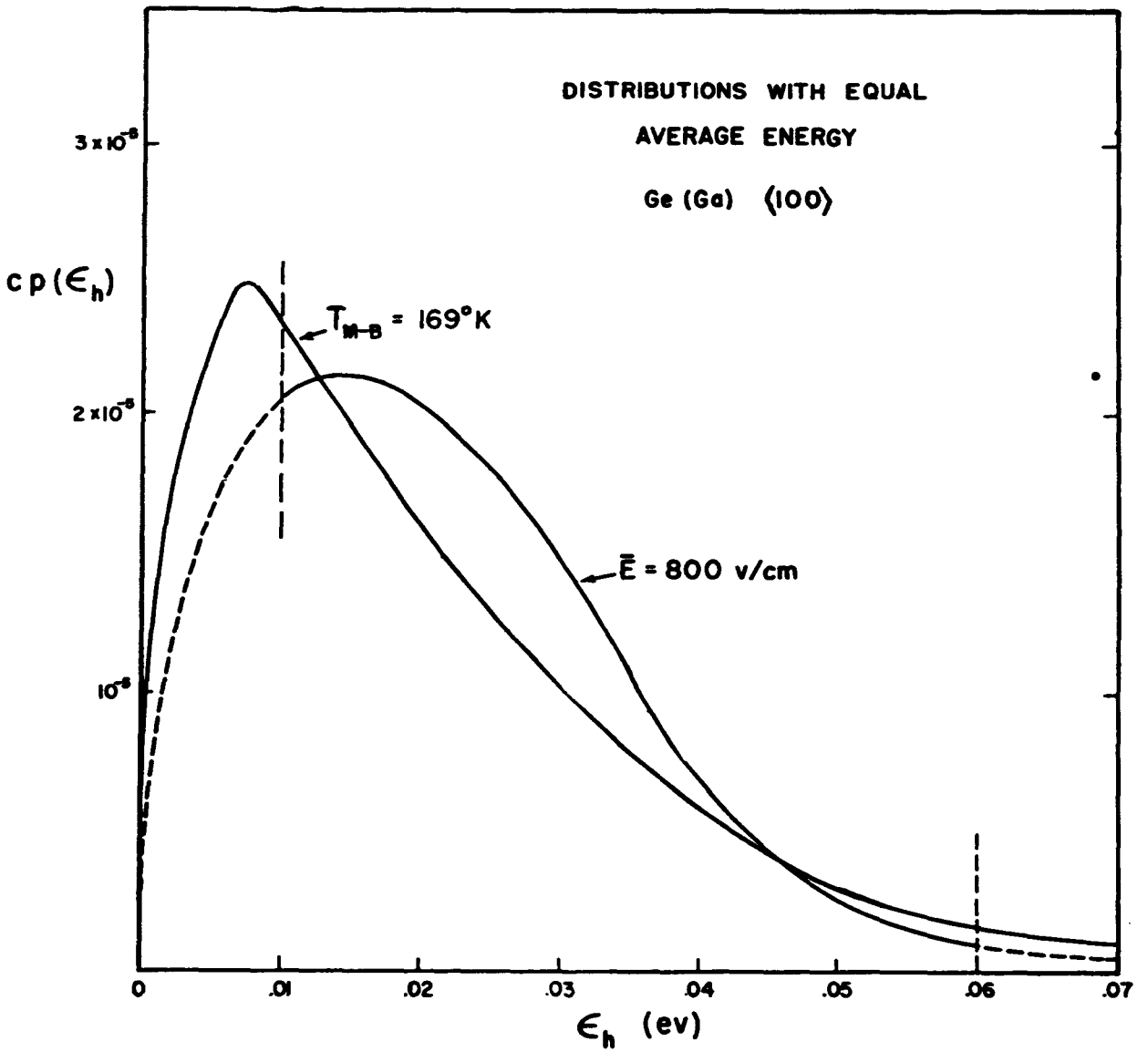
DISTRIBUTIONS WITH EQUAL
AVERAGE ENERGY
Ge (Ga) ⟨100⟩
3×10^{-5}
2×10^{-5}
10^{-5}
$cp(\epsilon_h)$
T_{M-B} = 169°K
$\bar{E}$ = 800 v/cm
0
.01
.02
.03
.04
.05
.06
.07
ϵ_h (ev)

FIGURE 6

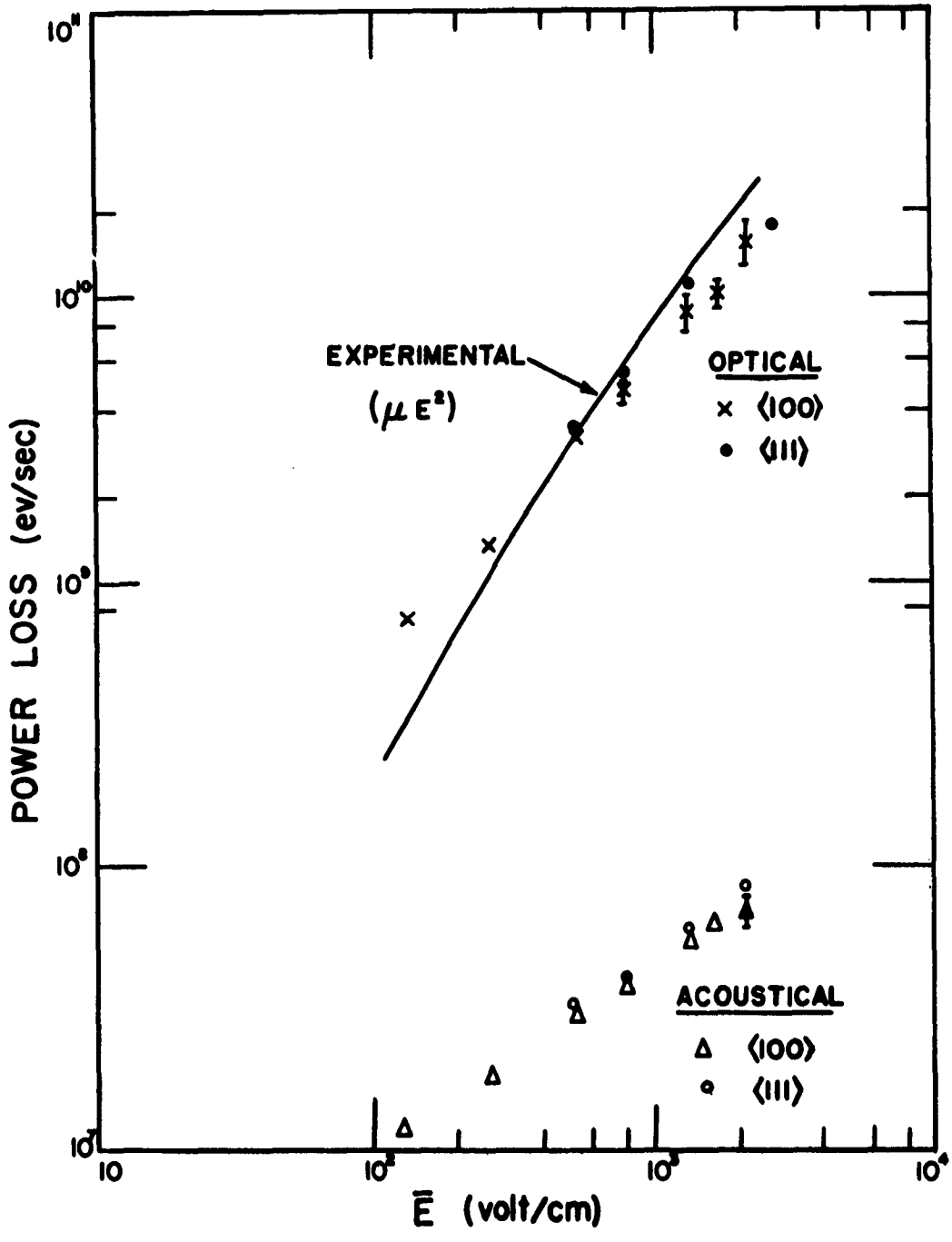
POWER LOSS (ev/sec)
10^{11}
10^{10}
10^{9}
10^{8}
10^{7}
10
10^{2}
10^{3}
10^{4}
$\bar{E}$ (volt/cm)
EXPERIMENTAL
(μE^2)
OPTICAL
× ⟨100⟩
• ⟨111⟩
ACOUSTICAL
Δ ⟨100⟩
○ ⟨111⟩

FIGURE 7

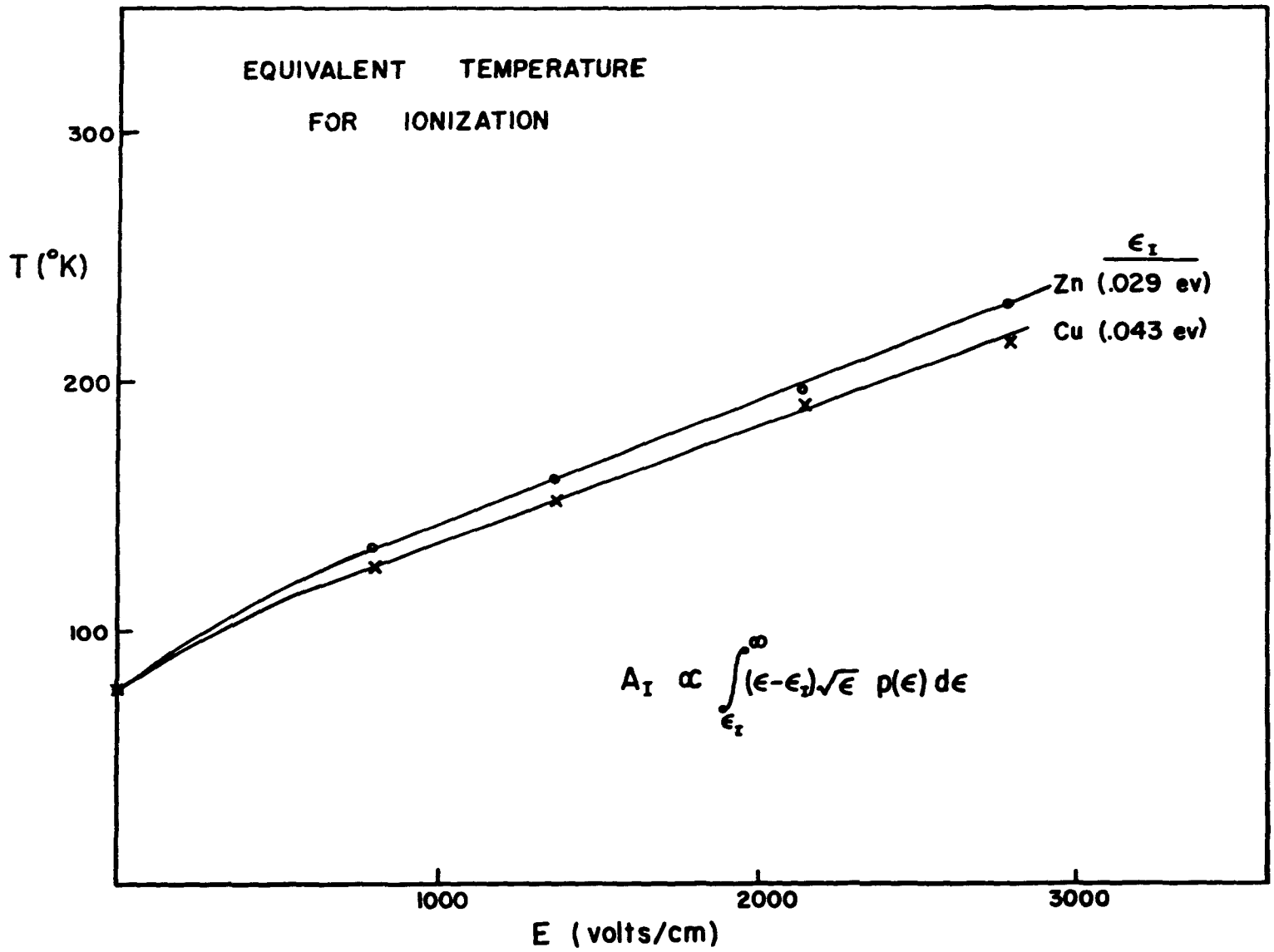
EQUIVALENT TEMPERATURE
FOR IONIZATION
T (°K)
300
200
100
1000
2000
3000
E (volts/cm)
$\frac{\epsilon_I}{}$
Zn (.029 ev)
Cu (.043 ev)
$A_I \propto \int_{\epsilon_I}^{\infty} (\epsilon - \epsilon_I)\sqrt{\epsilon}\ p(\epsilon)\, d\epsilon$

FIGURE 8

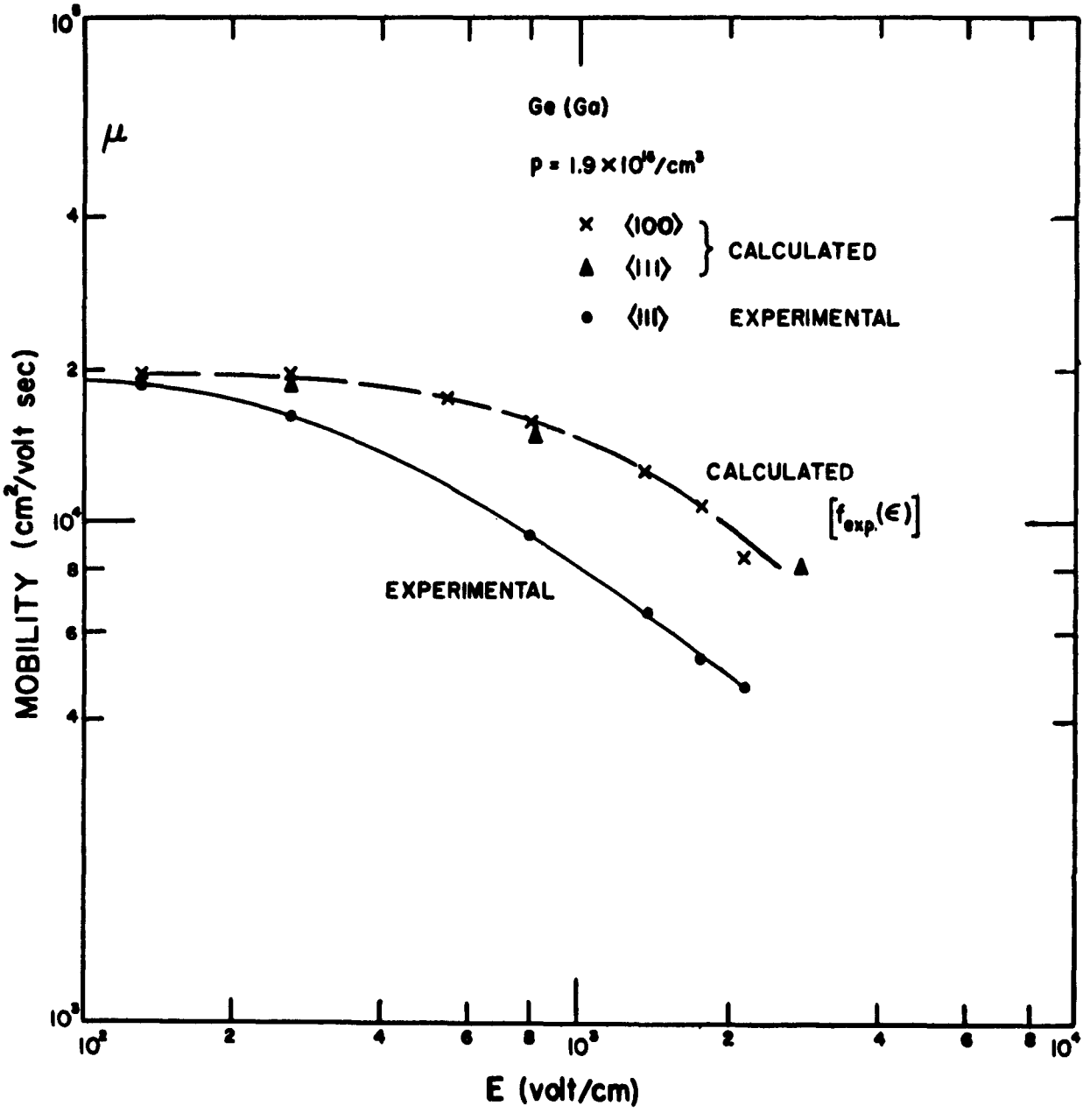
Ge (Ga)
p = 1.9 × 10^16/cm^3
μ
× ⟨100⟩
▲ ⟨111⟩
CALCULATED
• ⟨111⟩ EXPERIMENTAL
CALCULATED
[f_exp.(ϵ)]
EXPERIMENTAL
MOBILITY (cm^2/volt sec)
E (volt/cm)

FIGURE 9

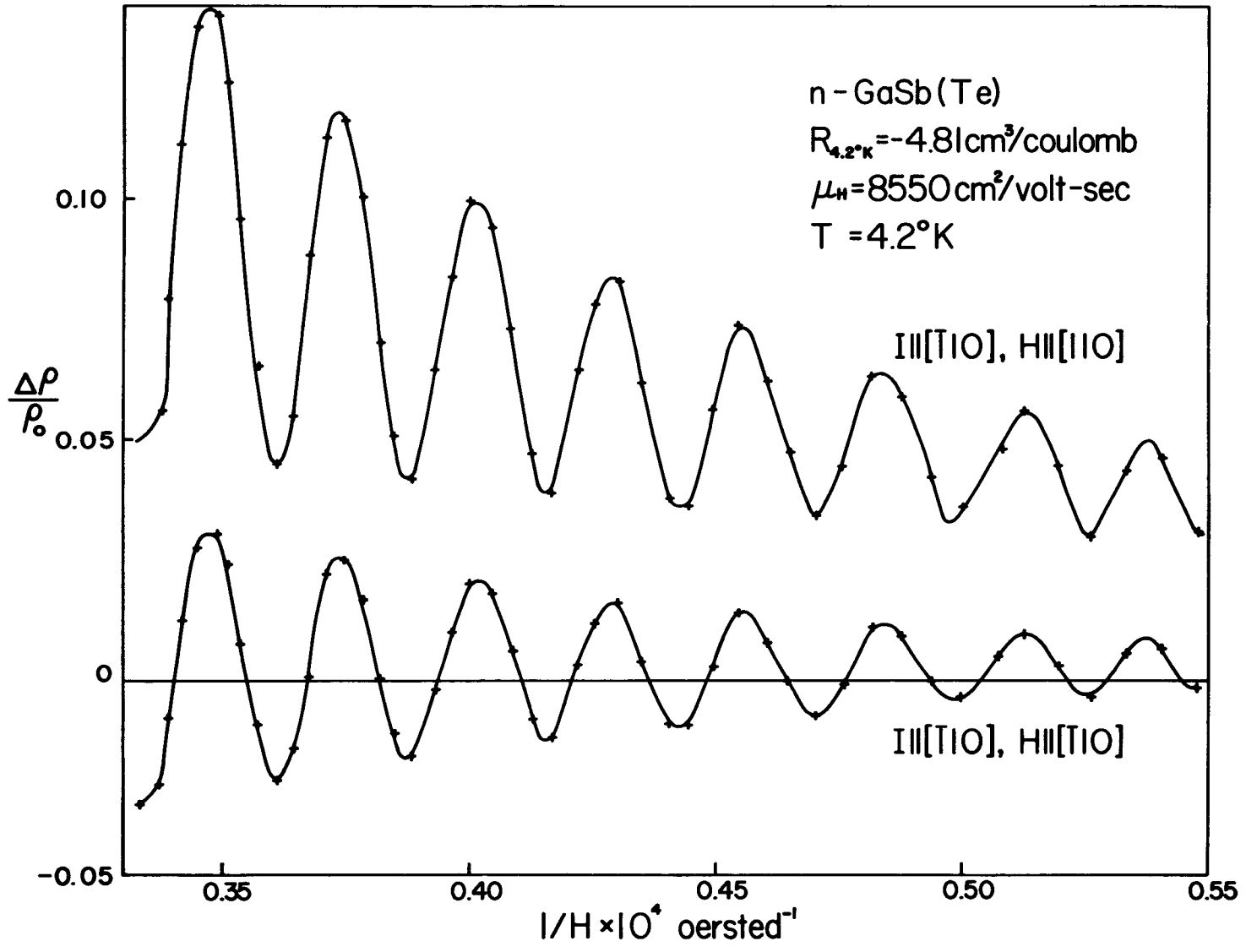
n - GaSb (Te)
$R_{4.2°K}$ = -4.81 cm³/coulomb
μ_H = 8550 cm²/volt-sec
T = 4.2°K
I||[110], H||[110]
I||[110], H||[110]
$\frac{\Delta\rho}{\rho_o}$
0.10
0.05
0
-0.05
0.35
0.40
0.45
0.50
0.55
1/H × 10⁴ oersted⁻¹

FIGURE 10

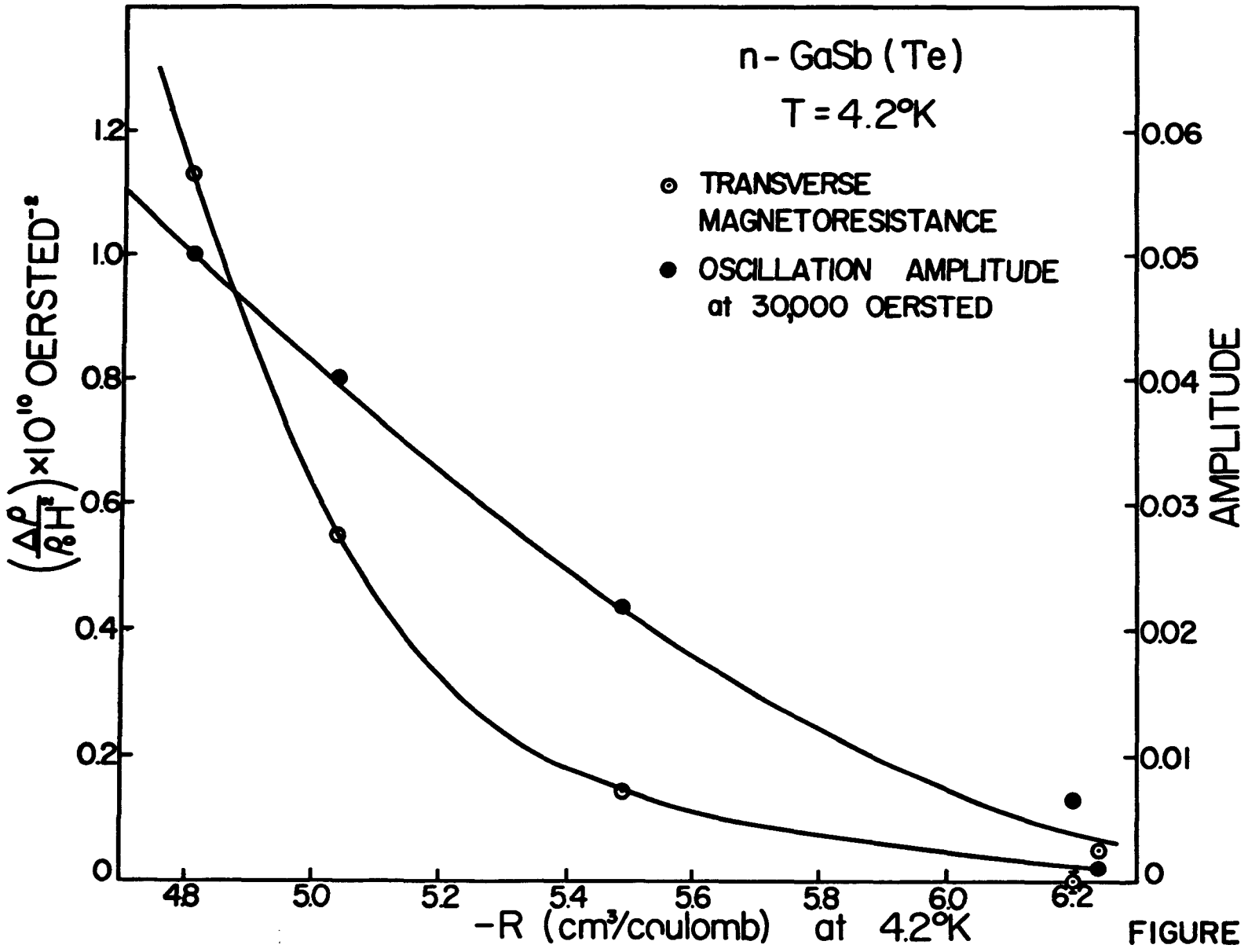
n - GaSb (Te)
T = 4.2°K
⊙ TRANSVERSE MAGNETORESISTANCE
● OSCILLATION AMPLITUDE at 30,000 OERSTED
$\left(\frac{\Delta\rho}{\rho H^2}\right)\times 10^{10}$ OERSTED^{-2}
AMPLITUDE
1.2
1.0
0.8
0.6
0.4
0.2
0
0.06
0.05
0.04
0.03
0.02
0.01
0
4.8
5.0
5.2
5.4
5.6
5.8
6.0
6.2
−R (cm³/coulomb) at 4.2°K

FIGURE 11

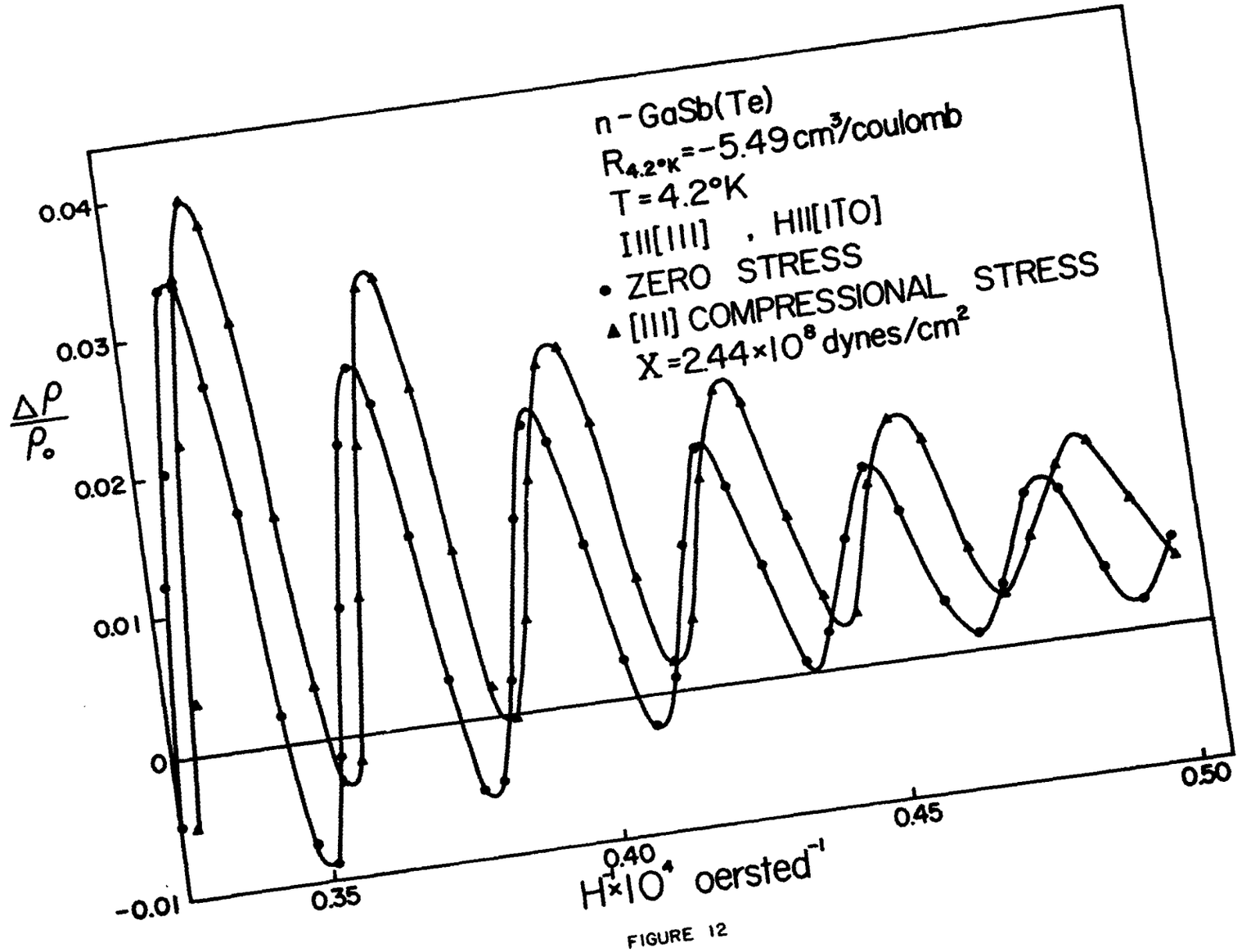
n-GaSb(Te)
$R_{4.2°K}$=-5.49 cm³/coulomb
T=4.2°K
I||[111] , H||[1TO]
• ZERO STRESS
▲ [111] COMPRESSIONAL STRESS
X=2.44×10⁸ dynes/cm²
0.04
0.03
0.02
0.01
0
-0.01
$\frac{\Delta\rho}{\rho_o}$
0.35
0.40
0.45
0.50
$H^{-1}\times10^{4}$ oersted^{-1}

FIGURE 12

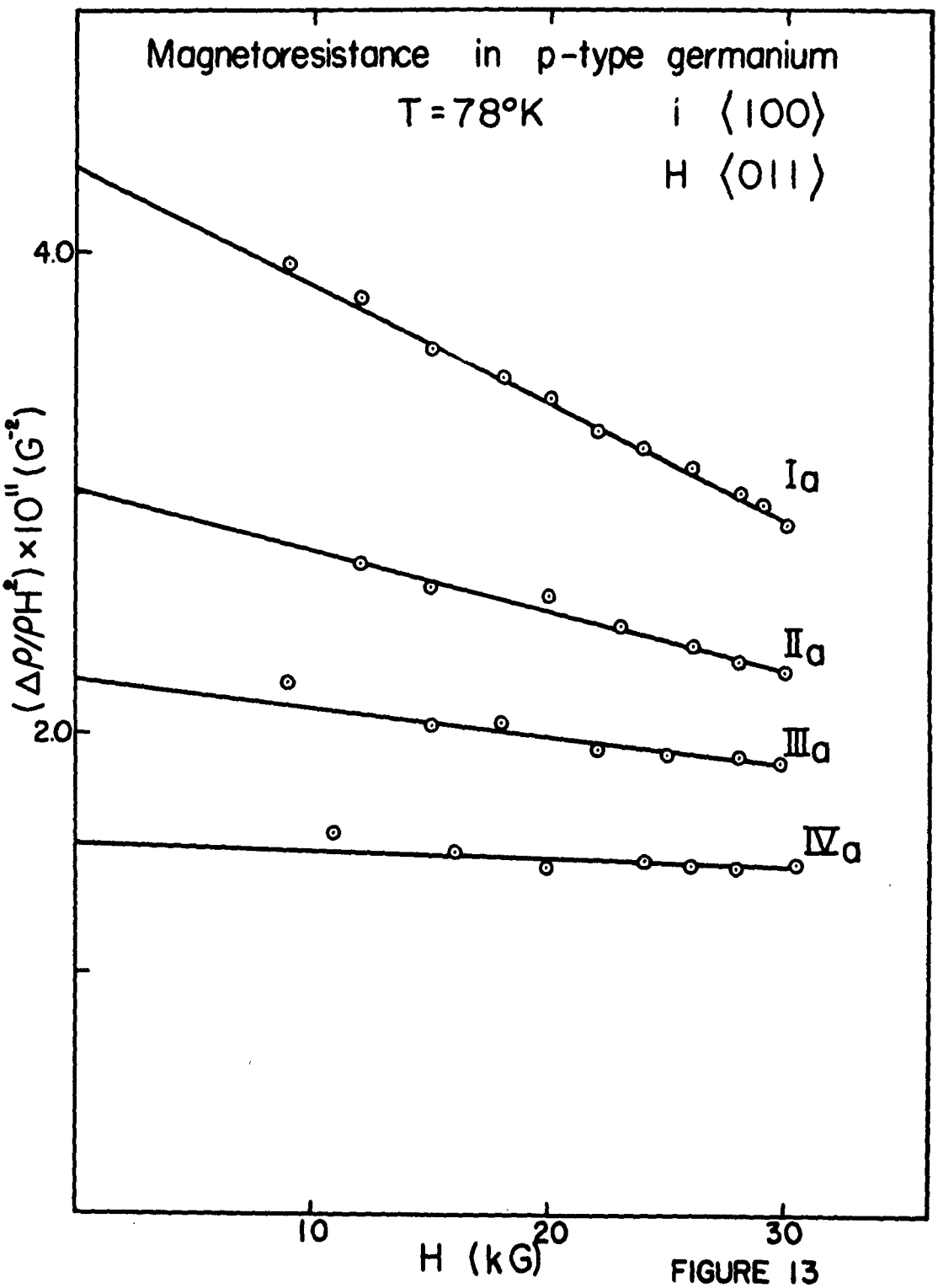
Magnetoresistance in p-type germanium
T = 78°K
i ⟨100⟩
H ⟨011⟩
4.0
2.0
$(\Delta\rho/\rho H^2) \times 10^{11} (G^{-2})$
Ia
IIa
IIIa
IVa
10
20
30
H (kG)

FIGURE 13

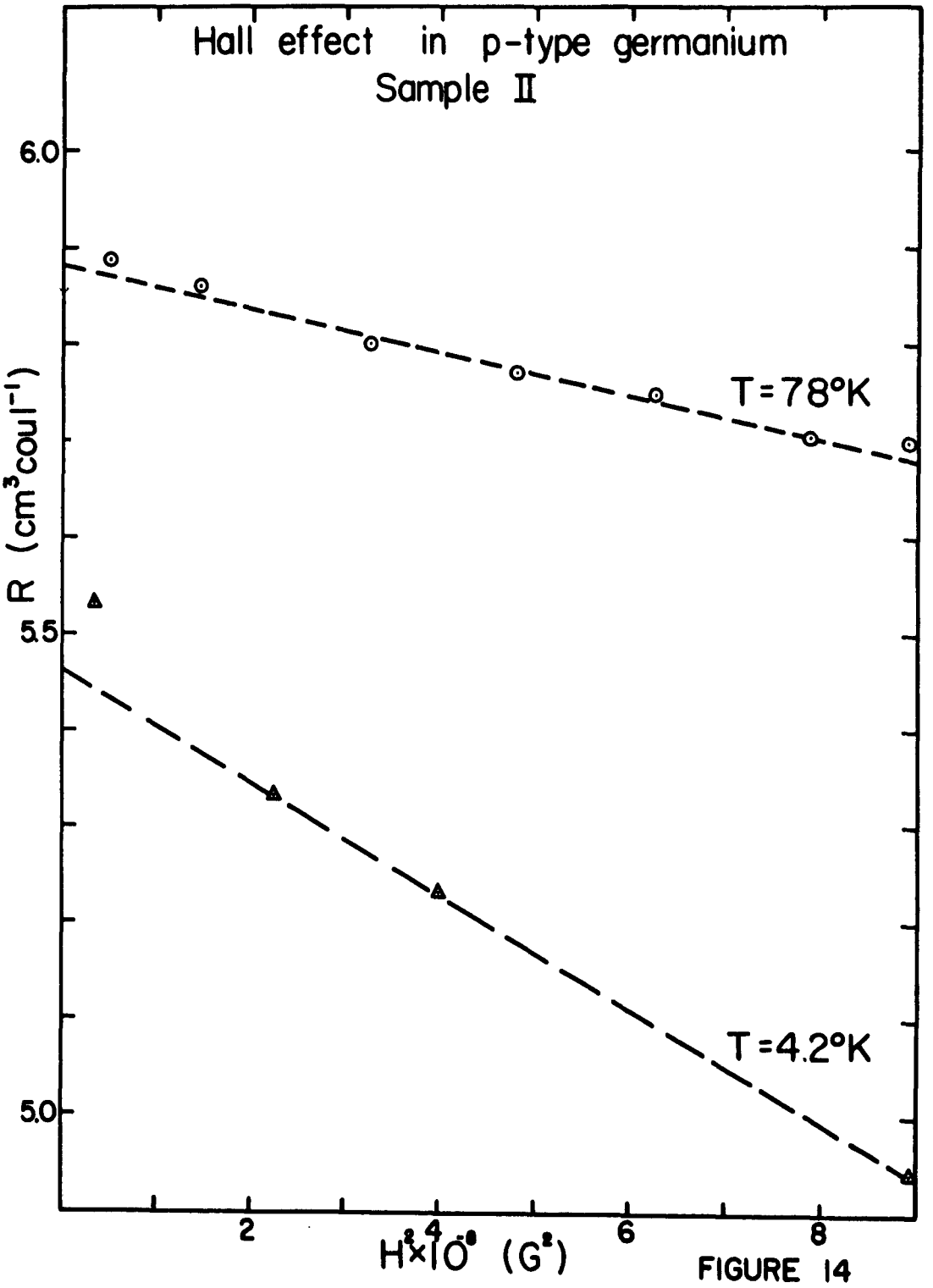
Hall effect in p-type germanium
Sample II
6.0
5.5
5.0
R (cm³coul⁻¹)
T=78°K
T=4.2°K
2
4
6
8
H²×10⁻⁸ (G²)

FIGURE 14

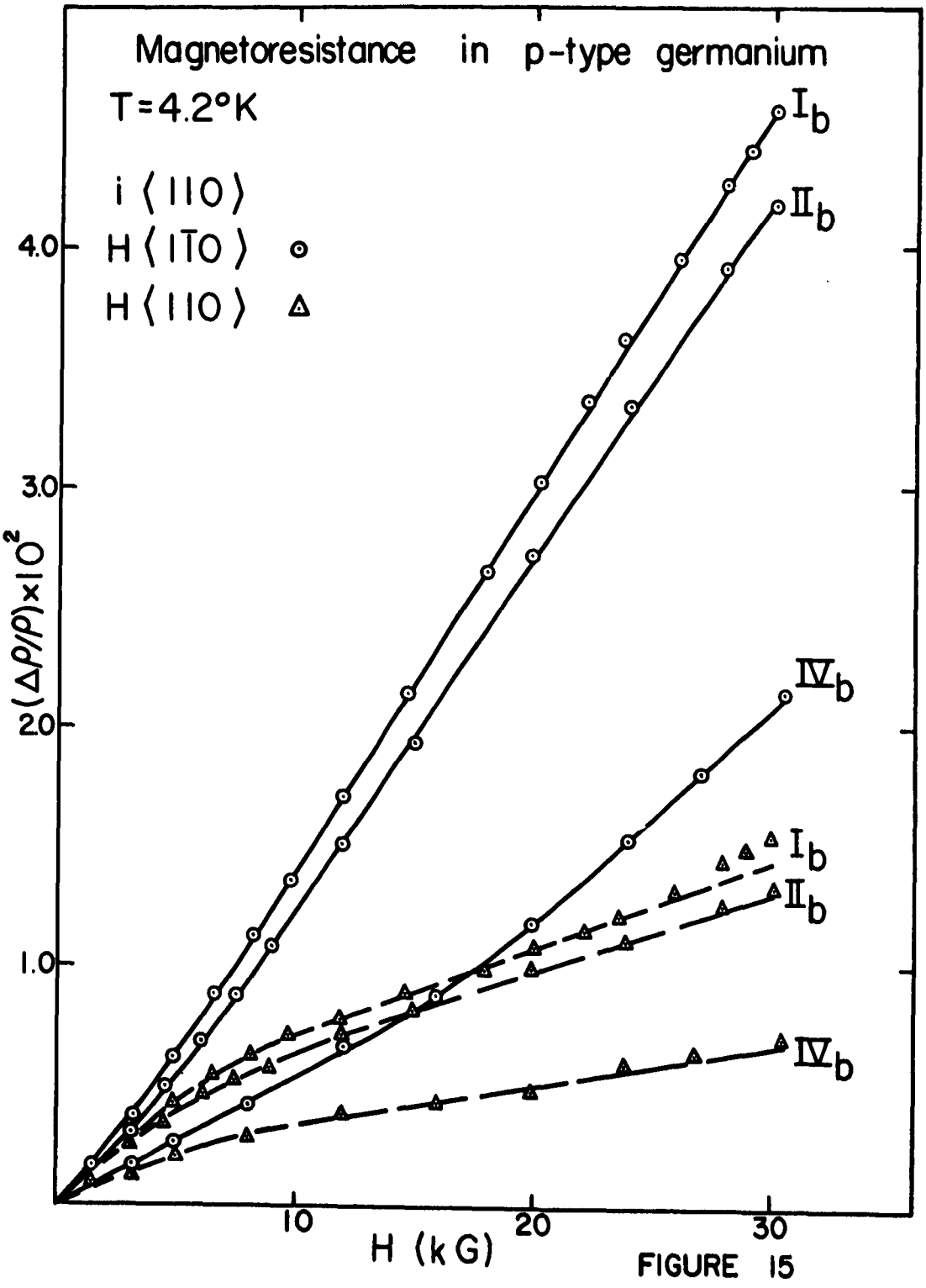
Magnetoresistance in p-type germanium
T=4.2°K
i ⟨110⟩
H ⟨1$\bar{1}$0⟩
H ⟨110⟩
I_b
II_b
IV_b
I_b
II_b
IV_b
4.0
3.0
2.0
1.0
$(\Delta\rho/\rho)\times10^2$
10
20
30
H (kG)

FIGURE 15

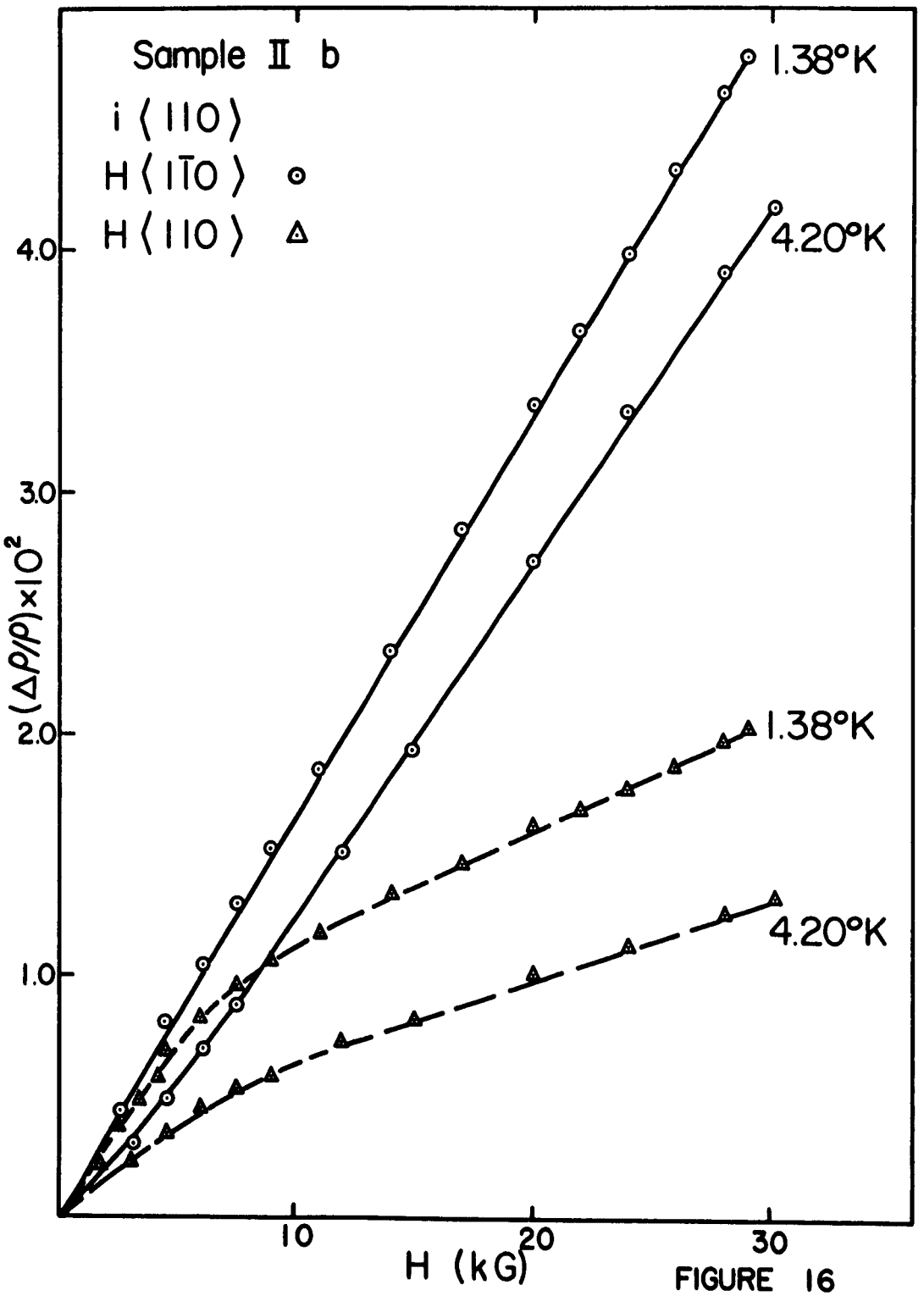
Sample II b
i ⟨110⟩
H ⟨1$\bar{1}$0⟩
H ⟨110⟩
1.38°K
4.20°K
1.38°K
4.20°K
4.0
3.0
2.0
1.0
$(\Delta\rho/\rho)\times10^2$
10
20
30
H (kG)

FIGURE 16

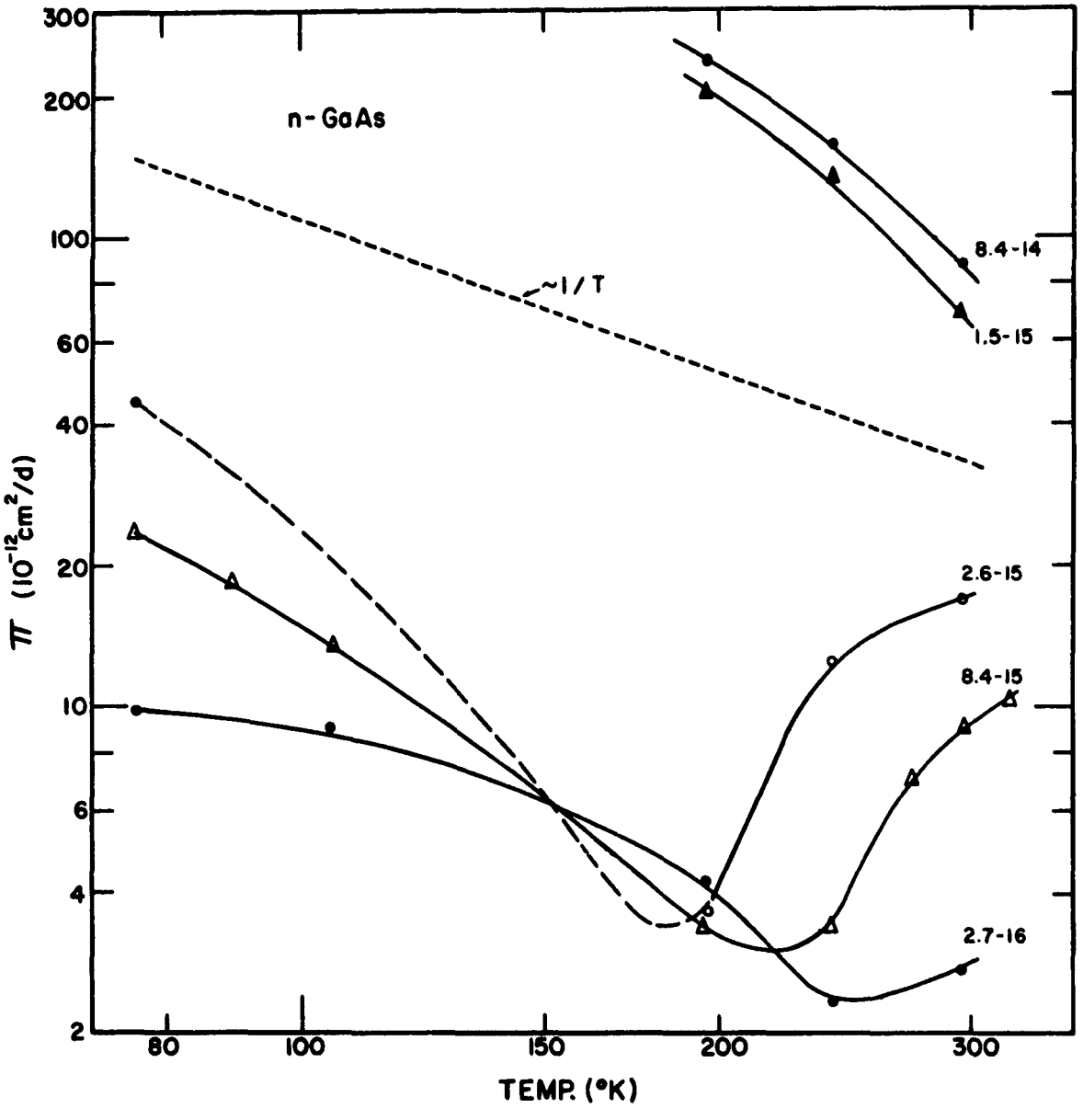
n-GaAs
~1/T
8.4-14
1.5-15
2.6-15
8.4-15
2.7-16
π (10⁻¹²cm²/d)
TEMP. (°K)
300
200
100
60
40
20
10
6
4
2
80
100
150
200
300

FIGURE 17

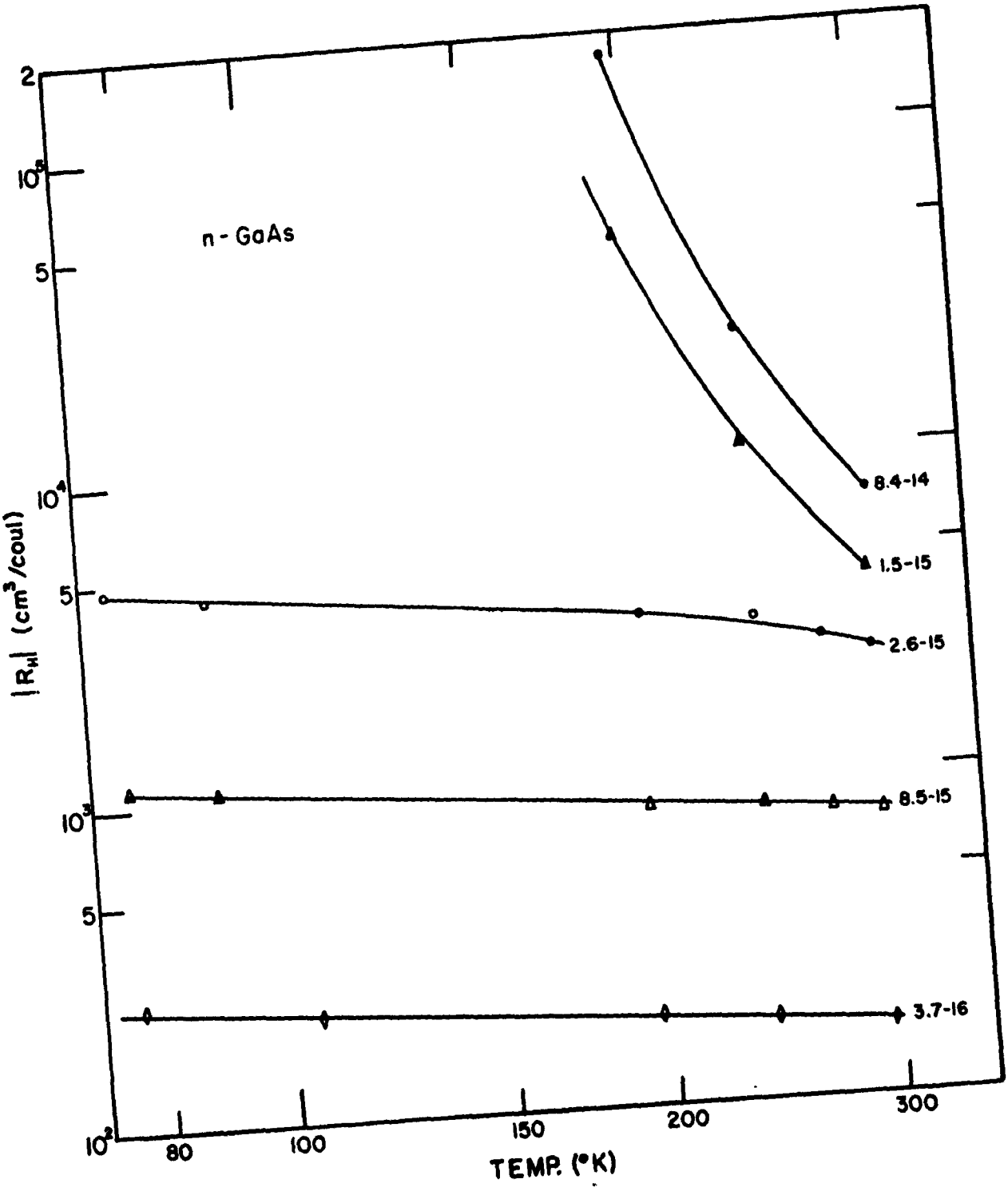
n - GaAs
8.4-14
1.5-15
2.6-15
8.5-15
3.7-16
$|R_H|$ (cm^3/coul)
TEMP. (°K)
2
10^5
5
10^4
5
10^3
5
10^2
80
100
150
200
300

FIGURE 18

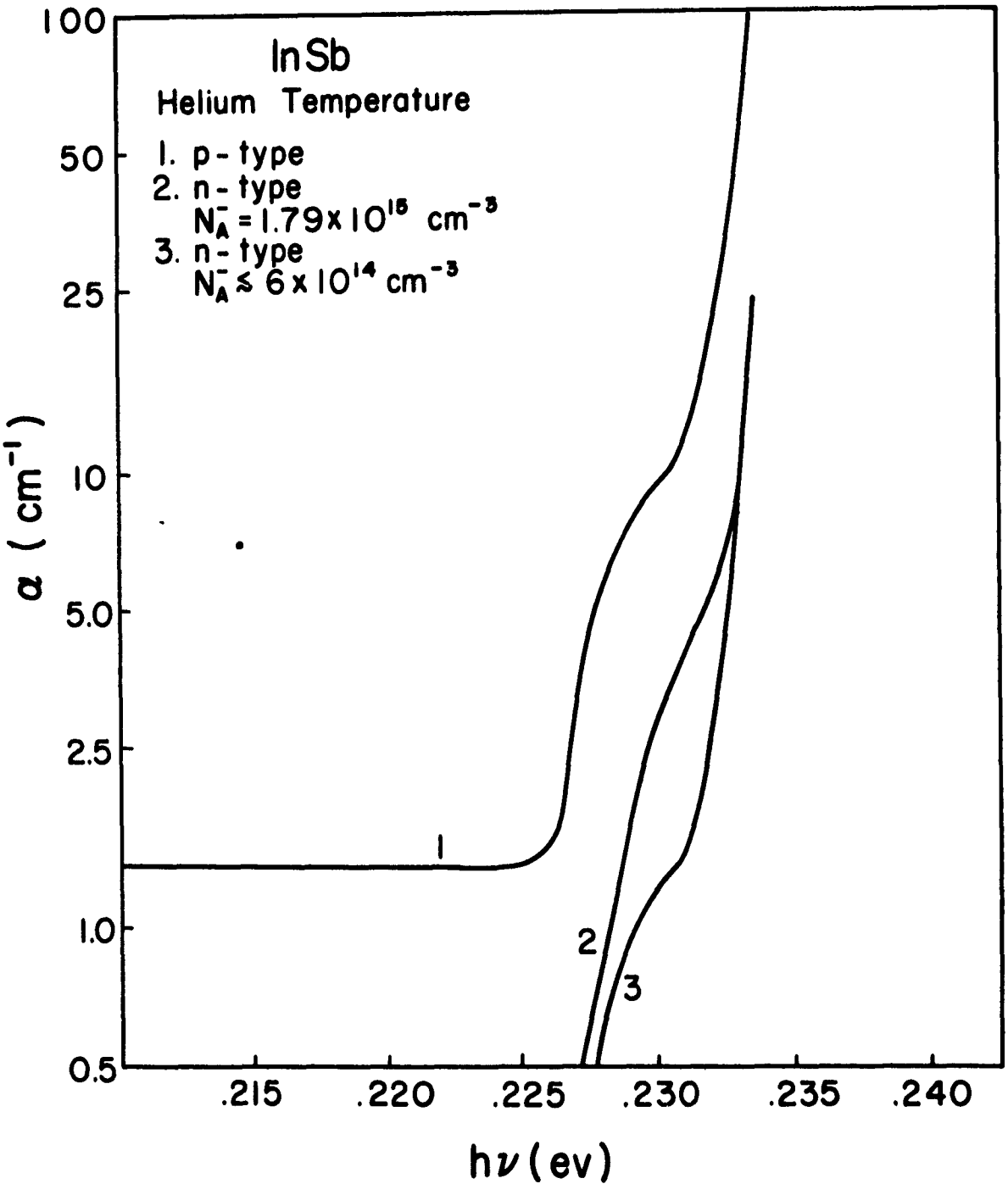
InSb
Helium Temperature
1. p-type
2. n-type
$N_A^- = 1.79 \times 10^{15}$ cm^{-3}
3. n-type
$N_A^- \lesssim 6 \times 10^{14}$ cm^{-3}
100
50
25
10
5.0
2.5
1.0
0.5
α (cm^{-1})
.215
.220
.225
.230
.235
.240
hν (ev)
1
2
3

FIGURE 19

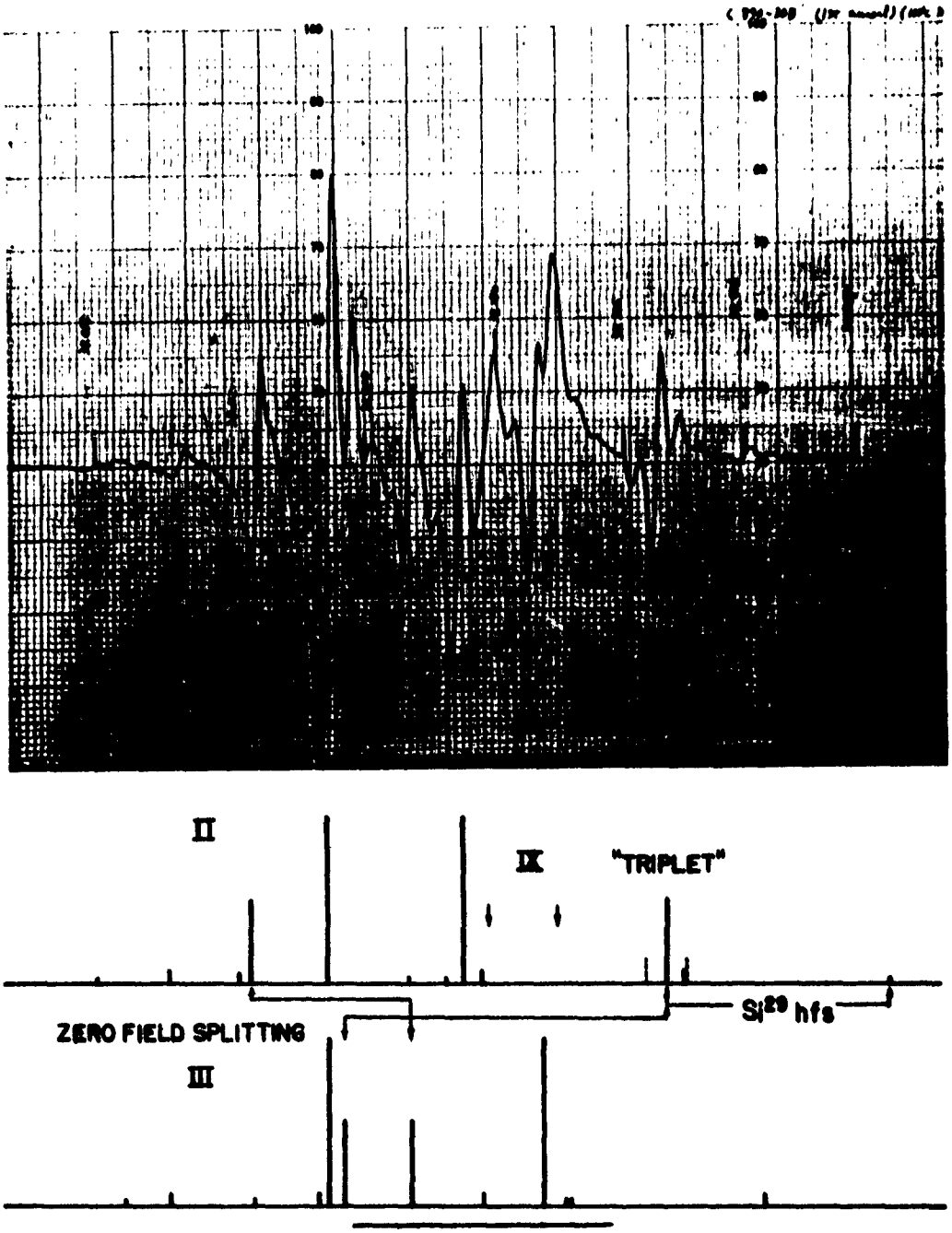

FIGURE 20

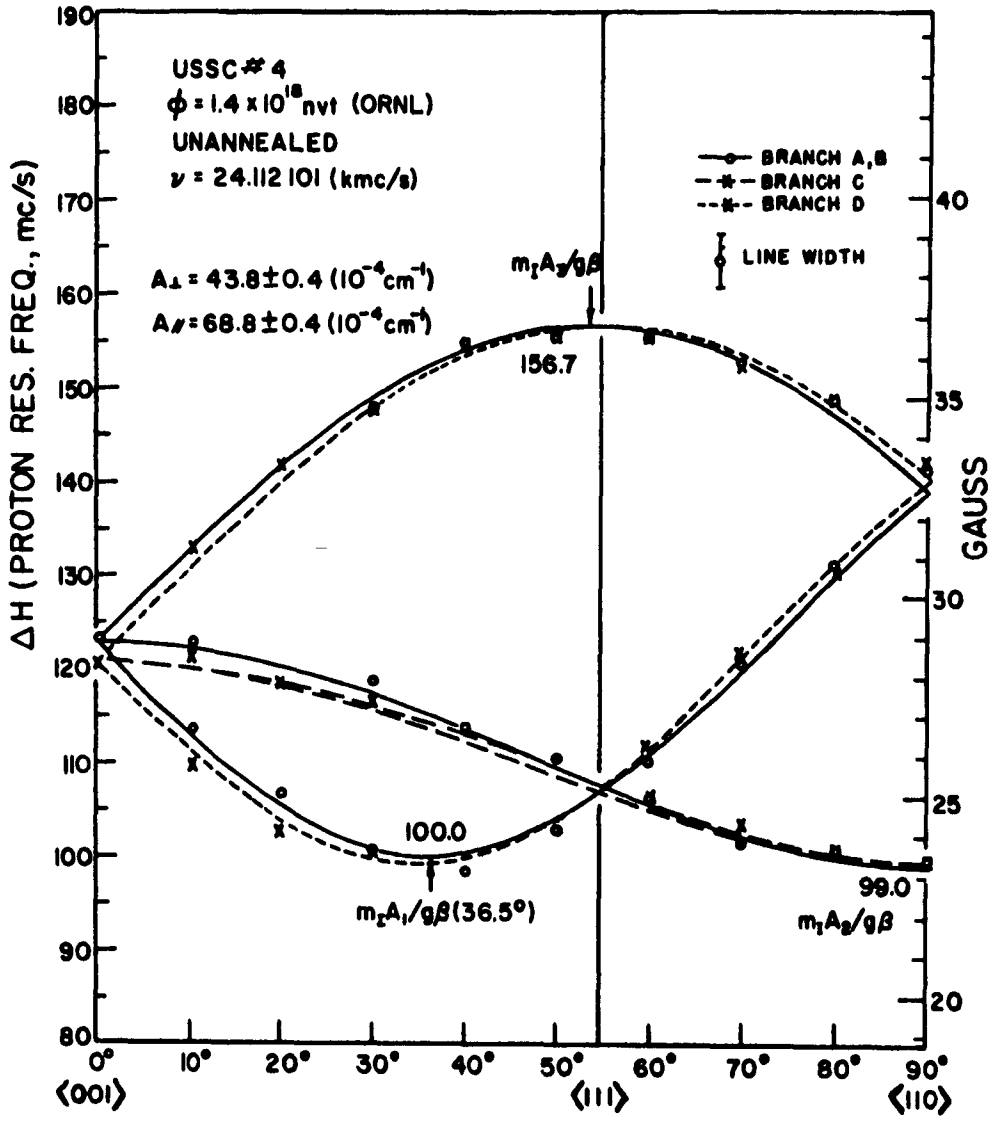

HYPERFINE SPLITTING OF CENTER (II, III)

FIGURE 21

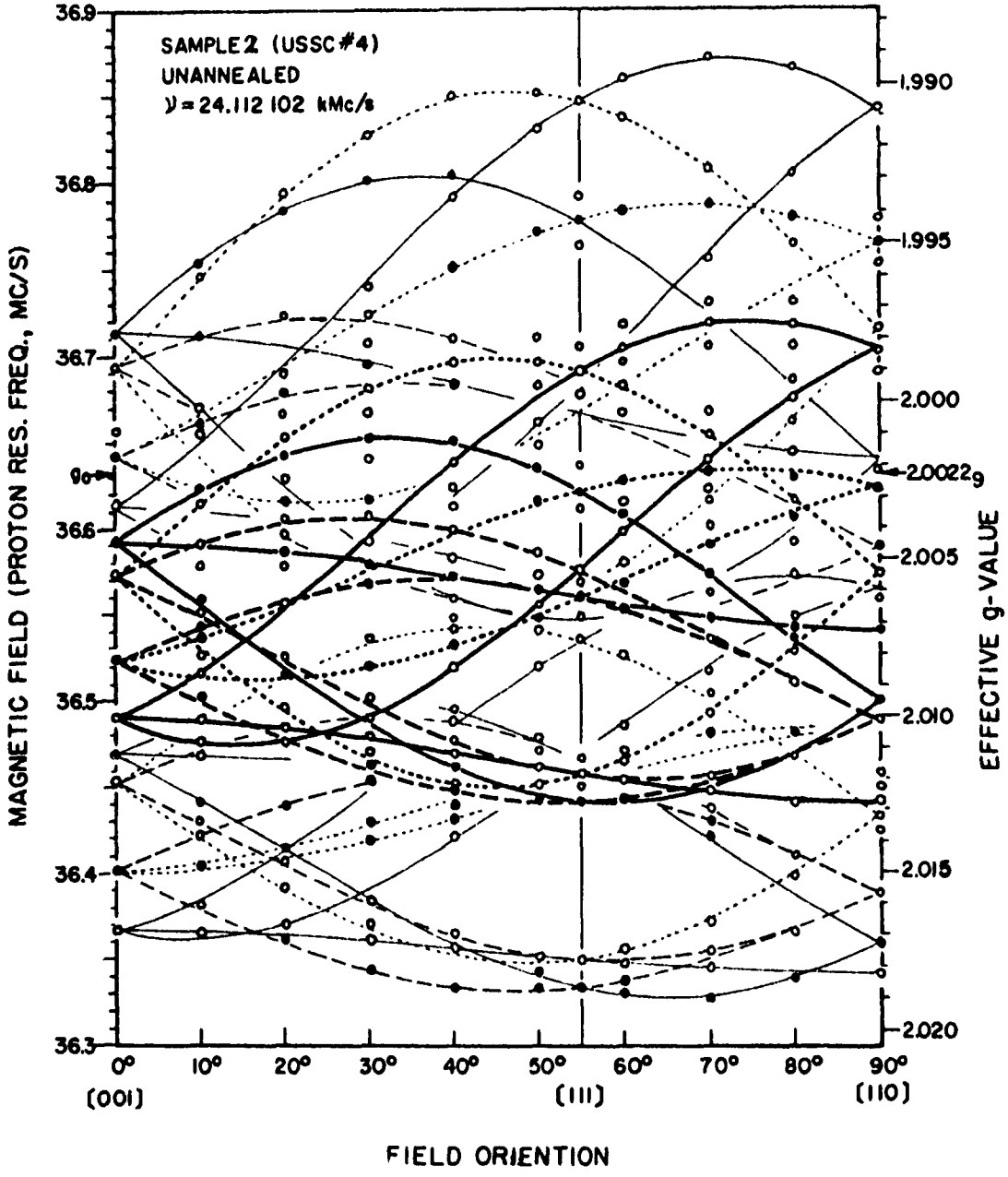
SAMPLE 2 (USSC #4)
UNANNEALED
ν = 24.112 102 kMc/s
MAGNETIC FIELD (PROTON RES. FREQ., MC/S)
EFFECTIVE g-VALUE
36.9
36.8
36.7
36.6
36.5
36.4
36.3
1.990
1.995
2.000
2.0022g
2.005
2.010
2.015
2.020
0°
10°
20°
30°
40°
50°
60°
70°
80°
90°
(001)
(111)
(110)
FIELD ORIENTION

FIGURE 22

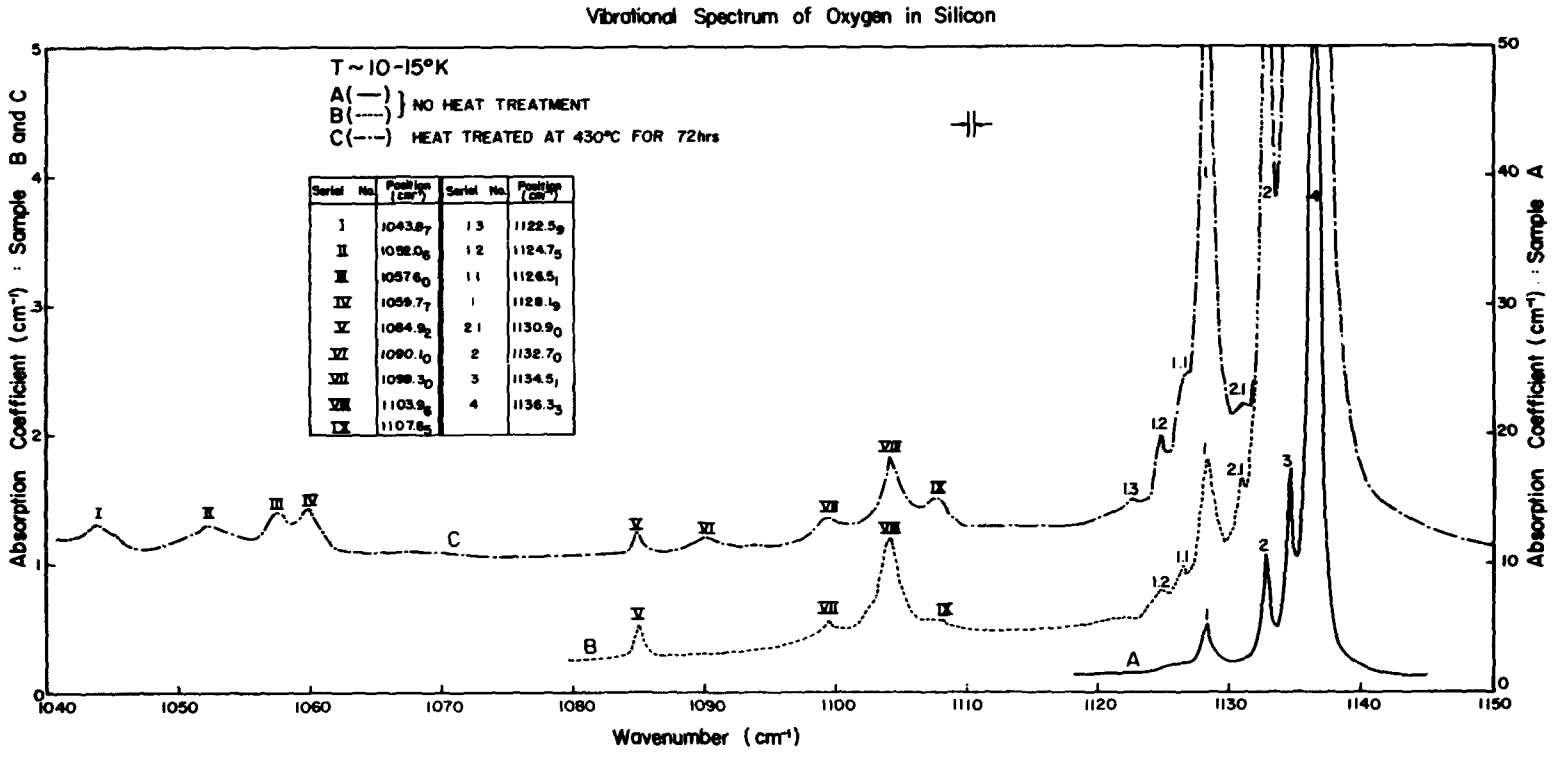

Serial No.	Position (cm^{-1})	Serial No.	Position (cm^{-1})
I	1043.8_7	13	1122.5_9
II	1052.0_6	12	1124.7_5
III	1057.6_0	11	1126.5_1
IV	1059.7_7	1	1128.1_9
V	1084.9_2	21	1130.9_0
VI	1090.1_0	2	1132.7_0
VII	1098.3_0	3	1134.5_1
VIII	1103.9_6	4	1136.3_3
IX	1107.6_5		

FIGURE 23

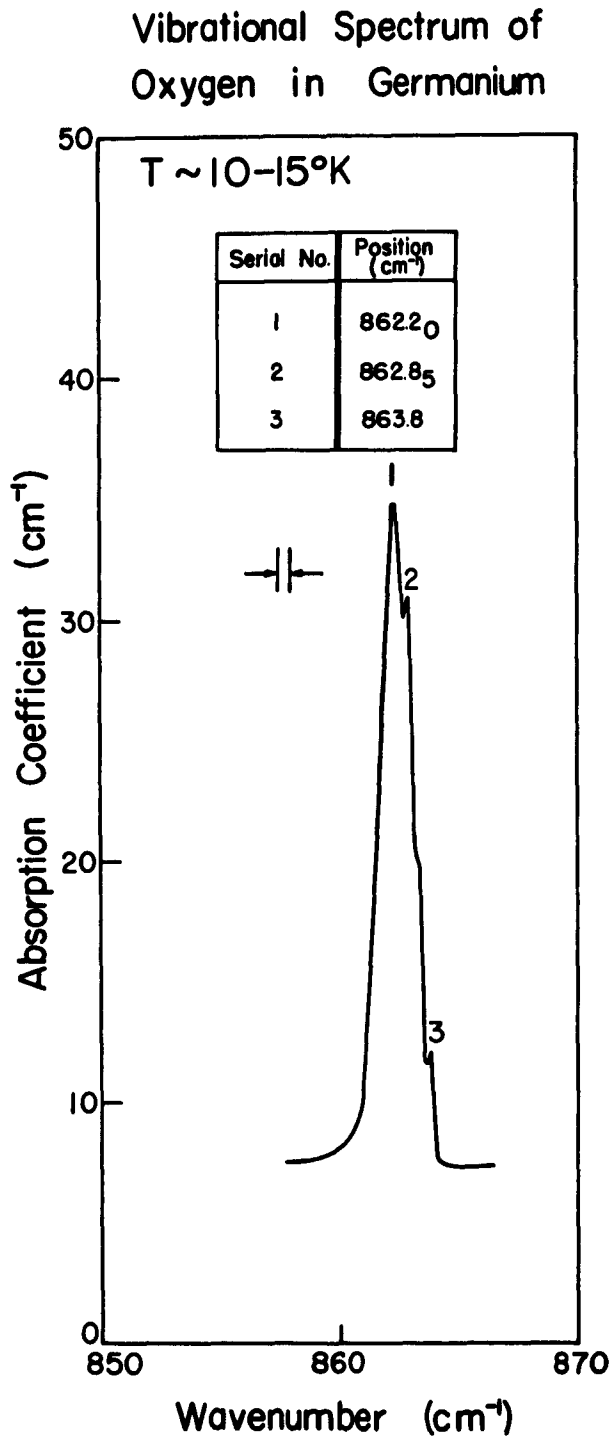
Vibrational Spectrum of
Oxygen in Germanium
T ~ 10-15°K
Serial No.
Position (cm⁻¹)
1
862.2₀
2
862.8₅
3
863.8
1
2
3
Absorption Coefficient (cm⁻¹)
0
10
20
30
40
50
850
860
870
Wavenumber (cm⁻¹)

FIGURE 24

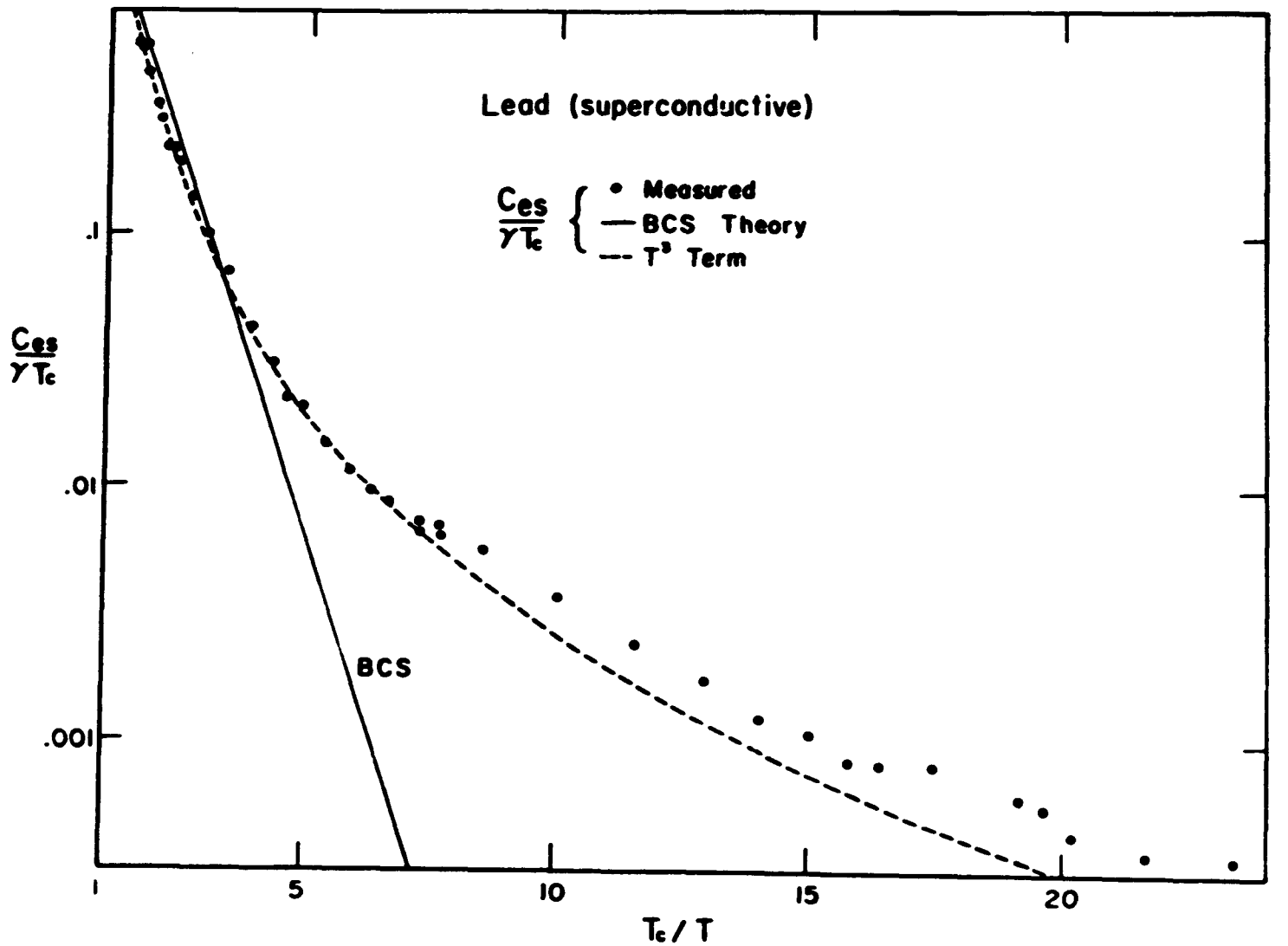
Lead (superconductive)
Ces/γTc
• Measured
— BCS Theory
--- T³ Term
Ces/γTc
.1
.01
.001
BCS
1
5
10
15
20
Tc / T

FIGURE 25

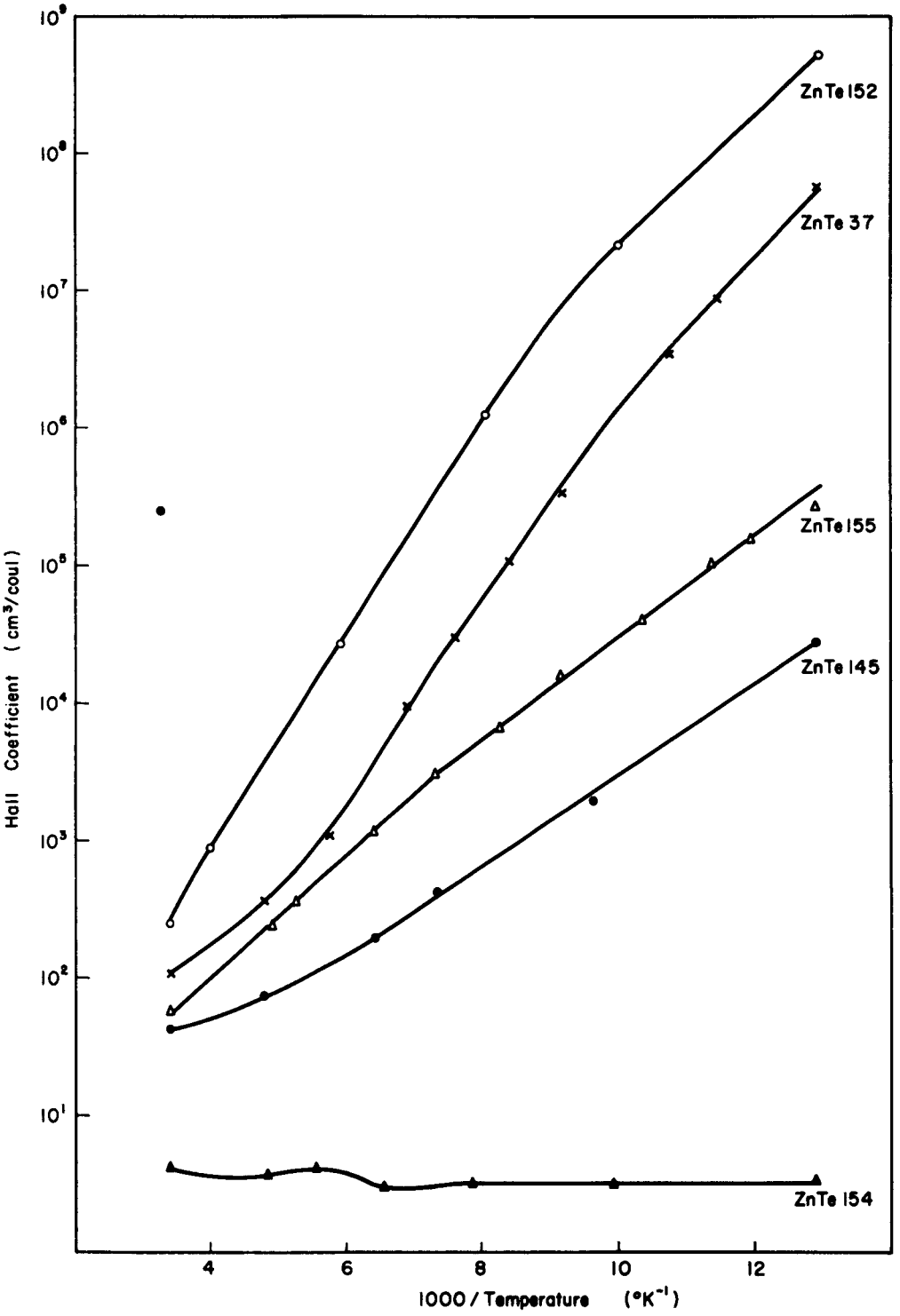
Hall Coefficient (cm³/coul)
10⁹
10⁸
10⁷
10⁶
10⁵
10⁴
10³
10²
10¹
ZnTe 152
ZnTe 37
ZnTe 155
ZnTe 145
ZnTe 154
4
6
8
10
12
1000 / Temperature (°K⁻¹)

FIGURE 26

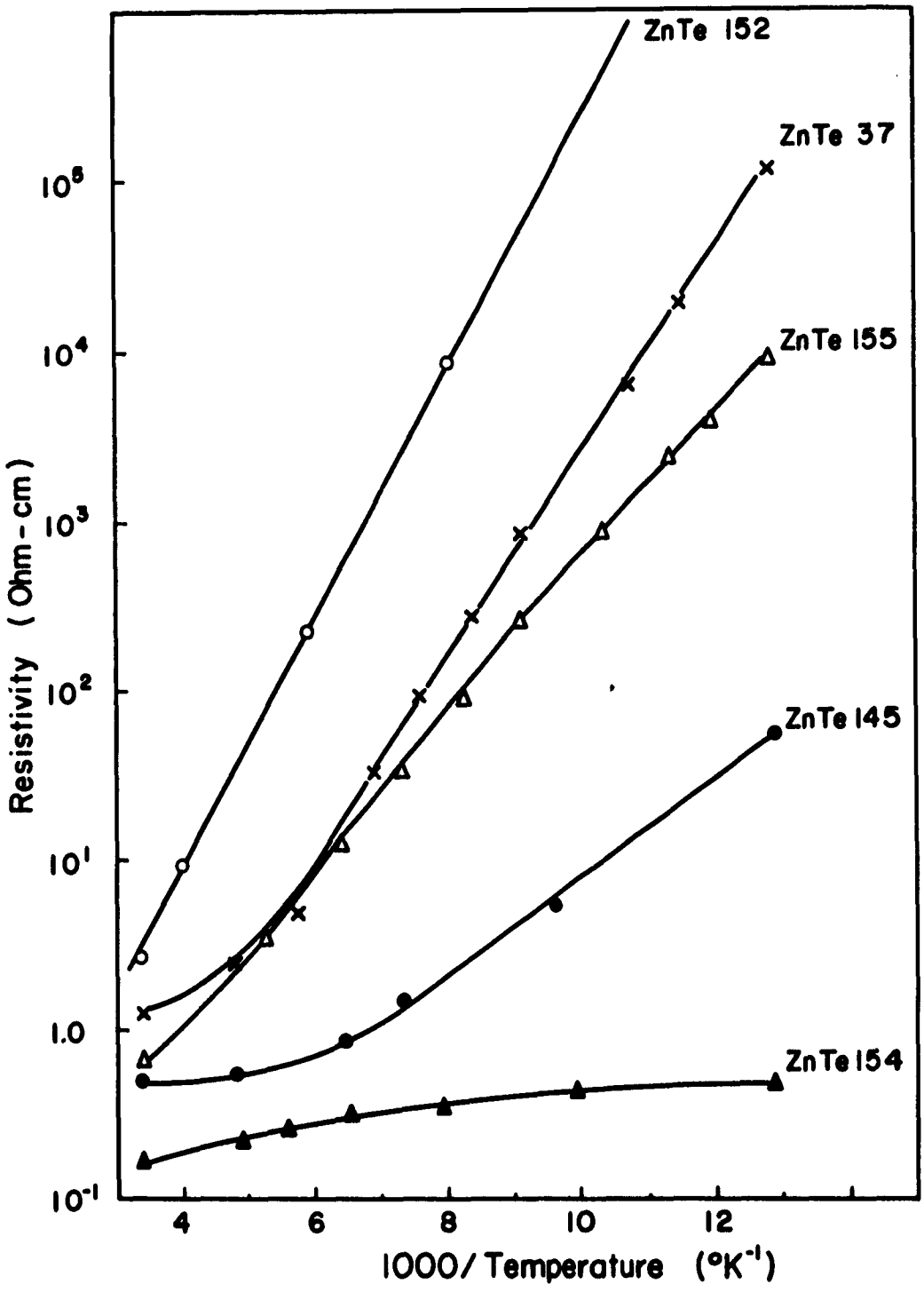
ZnTe 152
ZnTe 37
ZnTe 155
ZnTe 145
ZnTe 154
Resistivity (Ohm-cm)
10⁵
10⁴
10³
10²
10¹
1.0
10⁻¹
4
6
8
10
12
1000/ Temperature (°K⁻¹)

FIGURE 27

Distribution List

	No. of Copies
Director National Bureau of Standards Boulder, Colorado Attn: Radio Library	1
Commander, Air Force Command and Control Development Division Air Research and Development Command U. S. Air Force L. G. Hanscom Field Bedford, Massachusetts Attn: CRDTR 2E	1
Director U. S. Naval Research Laboratory Washington 25, D. C. Attn: Code 2027	1
Chief Signal Officer Department of the Army Washington 25, D. C. Attn: SIGRD	1
Commander Armed Services Technical Information Agency Arlington Hall Station Arlington 12, Virginia	10
Commander Wright Air Development Division Wright-Patterson Air Force Base, Ohio Attn: WCOSI-3 Attn: WCLKT-4	1 1
Department of the Navy Bureau of Ships Semiconductor Unit, Code 691A Washington 25, D. C. Attn: Mr. A. H. Young	1
Chief, Bureau of Ships Department of the Navy Washington 25, D. C. Attn: Code 327	1
Office of Naval Research Department of the Navy Washington 25, D. C. Attn: Code 427	1

DA 31-124-ARO(D)-17

	No. of Copies
Director U. S. Naval Research Laboratory Washington 25, D. C. Attn: Code 3560	1
Advisory Group on Electron Devices 346 Broadway New York 13, New York	2
Commanding Officer Watertown Arsenal Watertown, Massachusetts Attn: OMRO	1
Commander Air Research and Development Command Andrews Air Force Base Washington 25, D. C. Attn: RDRR-2	1
Commanding Officer U. S. Army Signal Electronics Research Unit Mountain View, California	1
Commandant Anti-aircraft Artillery and Guided Missile School Fort Bliss, Texas	1
U. S. Naval Inspector of Ordnance Applied Physics Laboratory Johns Hopkins University Silver Spring, Maryland	1
Donald K. Stevens Asst. Director for Metallurgy and Materials Programs Division of Research U. S. Atomic Energy Commission Washington 25, D. C.	1
New York Naval Shipyard Brooklyn 1, New York Attn: Material Laboratory, Code 912b	1
Naval Ordnance Laboratory Silver Spring, Maryland Attn: Solid State Division	1
Director, U. S. Naval Research Laboratory Washington 25, D. C. Attn: Code 6451	1

DA 31-124-ARO(D)-17

	No. of Copies
Commanding Officer and Director U. S. Naval Electronics Laboratory San Diego 52, California	1
Technical Library OASD (R and E) Rm 3E1065, The Pentagon Washington 25, D. C.	1
Chief of Ordnance Washington 25, D. C. Attn: ORDTX-AR	1
Commanding General U. S. Army Ordnance Missile Command Redstone Arsenal, Alabama Attn: ORDXM-DR	1
Commanding Officer Frankford Arsenal Philadelphia 37, Pennsylvania Attn: ORDBA-FEL	1
RADC (RAALD) Griffiss Air Force Base, New York Attn: Documents Library	1
Commanding Officer Diamond Ordnance Fuze Laboratory Connecticut Avenue and Van Ness Street Washington 25, D. C. Attn: T. T. Liimatainen	1
Commanding Officer U. S. Army Signal Equipment Support Agency Fort Monmouth, New Jersey Attn: SIGFM/ES-ASA	1
Army Liaison Office U. S. Naval Research Laboratory Washington 25, D. C.	1
Commander Rome Air Development Center Griffiss Air Force Base, New York Attn: RCRWE-3	1
Chief of Ordnance Washington 25, D. C. Attn: ORDTB-Materials	1

DA 31-124-ARO(D)-17

	No. of Copies
Continental Army Command Liaison Office U. S. Army Signal Research and Development Laboratory Fort Monmouth, New Jersey	1
U. S. Office of Naval Research National Bureau of Standards Corona, California	1
Commanding Officer U. S. Army Signal Research and Development Laboratory Fort Monmouth, New Jersey Attn: Technical Information Division FOR RETRANSMITTAL TO: Canadian Liaison Officer Office of the Chief Signal Officer Room 2B274, Pentagon Washington 25, D. C.	1
Commanding Officer Engineering Research and Development Laboratories Fort Belvoir, Virginia Attn: Technical Intelligence Branch	1
Battelle Memorial Institute 505 King Avenue Columbus 1, Ohio Attn: A. C. Beer	1
Chicago Midway Laboratories University of Chicago Chicago 37, Illinois Attn: Librarian	1
Technical Reports Collection 303A Pierce Hall Harvard University Cambridge 38, Massachusetts Attn: Librarian	1
Franklin Institute 20th Street and Benjamin Parkway Philadelphia, Pennsylvania	1
University of Illinois Urbana, Illinois Attn: Dr. J. Bardeen	1
Westinghouse Electric Corporation Youngwood, Pennsylvania Attn: R. K. Riel	1

DA 31-124-ARO(D)-17

	No. of Copies
Northwestern University Evanston, Illinois Attn: Dr. W. Nuxford	1
Chief of Research and Development OCS, Department of the Army Washington 25, D. C.	1
Hughes Aircraft Company Semiconductor Division P. O. Box 278 Newport Beach, California Attn: Library	1
National Bureau of Standards U. S. Department of Commerce Washington 25, D. C. Attn: P. J. Solgin	1
Philco Corporation "C" and Tioga Streets Philadelphia, Pennsylvania Attn: Mr. W. H. Forster	1
General Electric Company Semiconductor Products Department Electronics Park Syracuse, New York Attn: Dr. H. M. Sullivan, Advanced Semiconductor Lab.	1
Raytheon Company 150 California Street Newton, Massachusetts Attn: Mr. H. L. Gaudreau, Administrator Government Contracts	1
Bell Telephone Laboratories Murray Hill, New Jersey Attn: Mr. A. Anderson	1
Radio Corporation of America Harrison, New Jersey Attn: C. M. Bost	1
Brown University Providence 12, Rhode Island	1
Massachusetts Institute of Technology P. O. Box 73 Lexington 73, Massachusetts Attn: Library A-229	1

DA 31-124-ARO(D)-17	No. of Copies
Northwestern University Evanston, Illinois Attn: Dr. W. Nuxford	1
Chief of Research and Development OCS, Department of the Army Washington 25, D. C.	1
Hughes Aircraft Company Semiconductor Division P. O. Box 278 Newport Beach, California Attn: Library	1
National Bureau of Standards U. S. Department of Commerce Washington 25, D. C. Attn: P. J. Solgin	1
Philco Corporation "C" and Tioga Streets Philadelphia, Pennsylvania Attn: Mr. W. H. Forster	1
General Electric Company Semiconductor Products Department Electronics Park Syracuse, New York Attn: Dr. H. M. Sullivan, Advanced Semiconductor Lab.	1
Raytheon Company 150 California Street Newton, Massachusetts Attn: Mr. H. L. Gaudreau, Administrator Government Contracts	1
Bell Telephone Laboratories Murray Hill, New Jersey Attn: Mr. A. Anderson	1
Radio Corporation of America Harrison, New Jersey Attn: C. M. Bost	1
Brown University Providence 12, Rhode Island	1
Massachusetts Institute of Technology P. O. Box 73 Lexington 73, Massachusetts Attn: Library A-229	1

DA 31-124-ARO(D)-17

No. of Copies

University of Minnesota
Institute of Technology
Minneapolis 14, Minnesota
Attn: Dr. A. van der Ziel — 1

New York University
College of Engineering
University Heights
New York 53, New York
Attn: Dr. I. Cadoff — 1

Massachusetts Institute of Technology
Research and Development Laboratories
Cambridge 39, Massachusetts
Attn: Documents Office, Room 20B-221 — 1

Notre Dame University
Physics Department
South Bend, Indiana
Attn: Prof. J. C. Buch — 1

University of Michigan
Willow Run Research Center
Ypsilanti, Michigan
Attn: Librarian, IRIA — 1

Pennsylvania State University
College of Engineering and Architecture
University Park, Pennsylvania
Attn: S. H. Chamberlain, Librarian — 1

Sanders Associates, Inc.
Nashua, New Hampshire — 1

North American Aviation
International Airport
Los Angeles, California — 1

National Carbon Company
Division of Union Carbide Corporation
P. O. Box 6116
Cleveland, Ohio
Attn: Library — 1

Mr. Robert K. Willardson, Assistant Chief
Physical Chemistry Division
Battelle Memorial Institute
505 King Avenue
Columbus 1, Ohio — 1

DA 31-124-ARO(D)-17

	No. of Copies
Honeywell Research Center 500 Washington Avenue, South Hopkins, Minnesota Attn: Dr. Van W. Bearinger	1
Semiconductor Components Library Texas Instruments, Inc. P. O. Box 5012 Dallas 22, Texas	1
Stanford University Palo Alto, California Attn: Dr. John Moll, Electrical Engineering Department	1
Commander U. S. Naval Ordnance Test Station China Lake, California Attn: Code 5019	1
International Rectifier Corporation 1521 East Grand Avenue El Segundo, California Attn: Dr. C. A. Escoffery	1
Chief, U. S. Army Security Agency Arlington Hall Station Arlington 12, Virginia	2
Commanding Officer U. S. Army Research Office (Durham) Attn: CRD-AA-IP, Mr. Ulsh Box CH, Duke Station Durham, N. Carolina	3
Commanding Officer U. S. Army Signal Research and Development Laboratory Fort Monmouth, New Jersey	
Attn: Director of Research	1
Attn: Chief, Technical Documents Center	1
Attn: Chief, Technical Information Division	3
Attn: Exploratory Research Division "E"	1
Attn: Microwave Quantum and Electronics Br, Solid State and Frequency Control Div	1
Attn: Mr. P. Newman, Solid State and Frequency Control Div	3
Deputy President U. S. Army Security Agency Board Arlington Hall Station Arlington 12, Virginia	1

DA 31-124-ARO(D)-17

	No. of Copies
Sylvania Electric Products, Inc. Semiconductor Division 100 Sylvan Road Woburn, Massachusetts Attn: Mr. F. H. Bower	1
Diamond Ordnance Fuze Laboratories U. S. Army Ordnance Corps. Attn: ORD and L - 450-638 Mr. Raymond H. Comyn Washington 25, D. C.	1
Total number of copies to be distributed	- 100

This contract is supervised by the Institute for Exploratory Research
Scientific contact at Purdue: Dr. H. Y. Fan
Scientific contact at Signal R and D Laboratory: Dr. S. Benedict Levin
Telephone 201-535-1308